DISS. ETH No. 18368

IN VIVO MEASUREMENT OF TOTAL KNEE JOINT REPLACEMENT KINEMATICS AND KINETICS DURING STAIR DESCENT

A dissertation submitted to the
ETH ZURICH

for the degree of
DOCTOR OF SCIENCES

presented by
MAURO FORESTI
Dipl. El.-Ing. ETH
born on the 17th of December 1975
citizen of Lodrino, TI

accepted on the recommendation of
Prof. Dr. Edgar Stüssi, examiner
Prof. Dr. Robert Riener, co-examiner
Dr. Hans Gerber, co-examiner

2009

Abstract

Nowadays, advanced osteoarthritis of the knee is often treated by replacing the joint with a total knee arthroplasty. In order to optimize the implant to reflect the knee functionality as accurately as possible, a profound knowledge of the mechanisms acting in the knee is needed. Therefore, a through analysis of this complex articulation is inevitable.
For a complete biomechanical study of the human knee joint, accurate measurement systems become essential. Despite their popularity and state-of-the-art technology, video photogrammetric systems, commonly used in human movement analysis, are still prone to large errors introduced by soft tissue artifacts. Therefore, a great deal of work has been done to collect more accurate data of the knee joint by employing other measuring techniques such as video fluoroscopy.
In the past years, several approaches have been presented to overcome the limitation of the static field of view of conventional fluoroscopic systems by means of automated moving devices, thus allowing the biomechanical acquisition of level walking. However, more demanding tasks, such as stair descent, can bear serious difficulties for subjects that exhibit knee joint dysfunctions, including pain, strain and danger. Moreover, previous studies asserted, that stair descent is a motion task that needs to be considered in order to analyze and understand pathological or prosthetic knee movement patterns.

Consequently, the goal of this thesis was to acquire accurate kinematic and kinetic data of total knee arthroplasties during unconstrained stair descent by means of video fluoroscopy.

This manuscript is divided in the following four chapters:

Introduction. At first, this chapter provides the reader with background information about the human knee joint anatomy. It describes the main component that constitute the knee and briefly elucidates their functionality. This is followed by an overview about the history of total knee replacement and the related controversies that still persist nowadays. Thereafter, a concise review is given about the present available methods employed for the biomechanical study of the knee joint. The chapter ends with the formulation of the aim of this dissertation.

Experimental Methods. Presented in this chapter are the measuring systems that were utilized during this thesis.

A two degrees of freedom automated moving fluoroscopic system was developed. Furthermore, the imaging chain has been redesigned and enhanced to provide more flexibility and accuracy. A new instrumented stair case was built, and an advanced strategy for force measurement correction was assessed.

The outline of the measurements conducted during the thesis is drawn in the last section.

Experimental Results. This chapter reveals the results of the measurements carried out during this thesis. Two subjects were involved, one complaining about flexion disorders, the other one not. Video photogrammetry based results were compared to video fluoroscopic acquisitions (gold standard) with respect to knee joint rotations and moments.

Contradictory rotations were observed in the knee kinematics calculated by means of video photogrammetric data. The thereby resulting ranges of motion also differed significantly from the gold standard, but appeared to reproduce inter-subject discrepancies.

Despite overall absolute value disagreements, peak moments and moment trajectory patterns were reproduced quite well. Pathological patterns could clearly be observed for the subject affected by flexion disorders.

Synthesis. The thesis is wrapped up in this last chapter. A summary is presented with each finding drawn in the present work. A final outlook is given in the end.

Riassunto

Al giorno d'oggi, l'artrosi avanzata del ginocchio è frequentemente risolta attraverso una sostituzione dell'articolazione tramite un'artroplastica totale. Al fine di ottimizzare l'impianto per riprodurre la funzionalità del ginocchio più accuratamente possibile, è necessario che ci sia una profonda conoscenza dei meccanismi che agiscono nel ginocchio. Perciò, un'analisi approfondita di questa complessa articolazione è inevitabile.
Per un completo studio biomeccanico del ginocchio umano, è essenziale che si utilizzi accurati sistemi di misura. Nonostante la loro popolarità e attualità a livello scientifico, i sistemi video fotogrammetrici, ultilizzati comunemente nell'analisi del movimento umano, sono inclini a errori estesi introdotti dallo spostamento del tessuto. Quindi, molto lavoro è stato eseguito nel raccogliere accurati dati del ginocchio mediante l'utilizzo di altri sistemi di misura, quale la video fluoroscopia.
In passato, diversi approcci sono stati presentati per superare la limitazione statica del campo visivo dei sistemi di fluoroscopia convenzionali per mezzo di apparecchiature mobili ed automatizzate, permettendo così l'acquisizione biomeccanica del cammino. Ciò nonostante, compiti più esigenti, come la discesa di scale, possono nacondere delle serie difficoltà per soggetti che esibiscono delle disfunzioni al ginocchio, inclusi dolore, sforzo e pericolo. Inoltre, studi passati asserirono che la discesa di scale è un compito di moto che si deve considerare al fine di analizzare e capire modelli di movimento patologici.

Di conseguenza, l'obbiettivo di questa tesi fu di acquisire dati accurati sulla cinematica e cinetica di artroprotesi totale di ginocchio durante la discesa libera di scale per mezzo di video fluoroscopia.

Questo manoscritto è diviso nei quattro capitoli seguenti:

Introduzione. Per primo, questo capitolo offre informazioni di fondo sull'anatomia del ginocchio umano, ne descrive le componenti principali che lo costituiscono e delucida brevemente la loro funzionalità. In seguito, una veduta d'insieme sulla storia della sostituzione di ginocchio totale è illustrata con le relative controverse che persistono tuttoggi. Poi, una revisione concisa è data sui metodi disponibili e assunti per lo studio biomeccanico della giuntura del ginocchio. Il capitolo

finisce con la formulazione dello scopo perseguito durante questa dissertazione.

Metodi Sperimentali. Presentati in questo capitolo sono i sistemi di misurazione che sono stati utilizzati durante questa tesi.
Un sistema mobile di fluoroscopia fu sviluppato e dotato di automatizzazione su due gradi di libertà. Inoltre, la catena di formazione d'immagini fu riveduta e migliorata per offrire più flessibilità e accuratezza. Un nuova scala strumentata fu costruita con una strategia avanzata per la correzione della misurazione di forza.
Lo svolgimento delle misure condotte durante la tesi è descritto nell'ultima sezione di questo capitolo.

Risultati sperimentali. Questo capitolo rivela i risultati delle misure eseguiti durante questa tesi. Due soggetti furono coinvolti, uno con disturbi durante la flessione del ginocchio, e l'altro senza. I risultati basati sulla video fotogrammetria furono paragonati alle acqusizioni mediante video fluoroscopia le acquisizioni (parità aurea) con rispetto delle rotazioni e forze rotatorie del ginocchio.
Delle rotazioni contraddittorie furono osservate nella cinematica del ginocchio calcolate per mezzo di dati video fotogrammetrici. I risultanti raggi di moto differirono significativamente dalla parità aurea, ma apparvero essere in grado di riprodurre le discrepanze fra i soggetti.
Nonostante i disaccordi nei valore assoluti, i momenti massimi di rotazione e la loro traiettoria complessiva furono riprodotti piuttosto bene. Dei chiari motivi patologici furono osservati per il soggetto colpito da disturbi durante la flessione.

Sintesi. La tesi è ricapitolata in questa ultima parte. Un sommario è presentato con ogni scoperta raggiunta durante questo lavoro. Una prospettiva finale conclude il manoscritto.

Acknowledgements

During my dissertation, I benefitted from the help and support of many people around me and, therefore, I would like to express my heartfelt appreciation.

Many thanks go to Prof. Dr. Edgar Stüssi, my doctoral advisor. At first, he introduced me to the field of biomechanics and then, by making me part of his visions, he helped me find my own one and he leaded me successfully through my dissertation. Furthermore, I am very thankful to my supervisor Dr. Hans Gerber. He followed me very closely throughout all my time at the institute. He always guided me in the right direction, be it scientific, technical or social. Moreover, I also wish to thank Prof. Dr. Robert Riener for being co-referee for my dissertation. He believed in me from the first time we met, and I am very grateful for his invaluable advice.

I also would like to acknowledge all the members of Institute for Biomechanics and especially the following members. Dr. Alex Stacoff (†), Dr. Jachen Denoth, Dr. Silvio Lorenzetti, Prof. Dr. Ralph Müller, Sofia Delamanis and Kathrin Palmer. I also would like to truly thank the members of the I^2T-group, especially Peter Schwilch and Marco Hitz. Firstly, because they are able to constantly put up with my southern temper. Secondly, because they always manage to calm me down and bring me back to the ground. And finally, because of their great technical knowledge and support, they helped me realize the present work. Furthermore, I am very grateful to *the Lasts of the Mohicans*, Urs Stöcker, Renate List and Daniel Baumgartner, with whom I madly shared the never-ending sleepless moments of the final *rush fever*.
My gratitude goes also to the RMS foundation in Bettlach for their financial support, to Mathys AG Bettlach and Philips Medical Systems for their technical support.

To the *Wagi-wagis* and close friends, I am very grateful because they always give me a reason to disconnect, blow off steam and laugh my butt off.

A big thank goes to my family and especially my mother, for being there for me since I took the first steps into my life and for helping me growing up to the man I am now.

Last but for shure not least, I want to express all my deep gratitude to Dominique, for all the love and understanding, for always standing there by me and letting me be who I am, for supporting my crazy ideas and finally for bringing so much color into my life.

Contents

Abbreviations

2D	two dimensional
3D	three dimensional
ACL	Anterior cruciate ligament
BAPI36	72 year old male participating in the study
BV	Bildverstärker (image intensifier)
CAD	Computer aided design
CCD	Charge-coupled device
COP	Center of pressure
CT	Computer tomography
DRR	Digital reconstructed radiograph
FELE30	78 year old female participating in the study
GRF	Ground reaction forces
IfB	Institute for Biomechanics
LCL	Lateral collateral ligament
MCL	Medial collateral ligament
MRI	Magnetic resonance imaging
PCL	Posterior cruciate ligament
RMSE	Root mean squared error
TKA	Total knee arthroplasty

It is shameful for man to rest in ignorance of the structure of his own body, especially when the knowledge of it mainly conduces to his welfare, and directs his application of his own powers.

Melanchthon (1497 - 1560)

1 Introduction

Articulations are very complex parts of our body that enable us to perform movements in space with extreme flexibility and perfection. They are involved in daily tasks such as absorbing shocks, coordinating whole body motions, and allowing for extensive rotations between body segments. Furthermore, they can be stabilized, thus inhibiting the body from collapsing.
The main components of a joint such as the knee are bones, ligaments, cartilage, muscles and tendons. They are positioned, shaped and structured to build a stable and very compact complex for interactions between body segments, which are preserved over time. However, injuries or illness can disrupt this subtle balance, hence altering, i.e. deteriorating the whole structure and functionality of the articulation. This condition, also referred to as osteoarthritis, provides discomfort and under circumstances also severe pain. In order to reduce, postpone or even prevent this type of joint collapse, it is essential to fully understand the mechanisms ruling in this complex structure.

1.1 Anatomy of the Human Knee Joint

In this section, a brief overview of the knee anatomy and its relevance to the joint functionality is given. Furthermore, the reader is referred to figure 1.1, 1.2 and 1.3 for a visual representation of the knee anatomy.

1.1.1 Bones

The knee is classified as a diarthrodial joint[1]. Two long bones, the femur and the tibia, and an oval shaped, sesamoid bone[2], the patella, constitute the main part of knee and are connected together to form three specific articulation compartments: the patellofemoral compartment and the medial and lateral femorotibial compartments. The femur divides distally into two condyle, which are separated by the intercondylar notch. The medial femoral condyle is longer and larger than the lateral femoral condyle and has a greater radius of curvature [113]. At full extension, the lateral condyle ironically exhibits a slightly wider contact area than the medial condyle.
At the level of the tibiofemoral articulation, the tibia forms proximally into the tibial plateau and is divided by the lateral and medial tibial eminences[3] into two separate condyles. The medial condyle extends more anteroposteriorly than the lateral condyle and has a clear concave shape, whereas the lateral condyle exhibits a rather convex curvature in the parasagittal projection. Both tibial condyles slope posteriorly.
Extending posteriorly to the femoral intercondylar notch, the patellofemoral groove, also known as femoral sulcus, articulate with the posterior surface of the patella to form the patellofemoral joint.
The fibula is anteriorly connected to the tibia by syndesmosis and does not actually constitute an articulating part of the knee joint.

1.1.2 Ligaments

Ligaments are connective tissue that guide and constrain the movement of articulating bones. Although they are innervated for sensory purposes [58], their contribution to motion is merely passive.

The femur is connected to the tibia by four major ligaments: the medial and lateral collateral ligaments (MCL and LCL) and the anterior and posterior cruciate ligaments (ACL and PCL). The collateral ligaments are extra-articular, whereas the cruciate ligaments are intra-articular but still extra-synovial.
The MCL originates from the medial femoral epicondyle at the adductor tubercle and descends distally and fans out as it inserts into the medial tibial metaphisis. The MCL has recently been rationalized into three main structures: the longitudinal fibres of

[1] A joint is defined as a diarthrosis, when the surfaces of two skeletal parts are free to articulate with one another.

[2] A bone embedded in a tendon

[3] Protrusions of bone

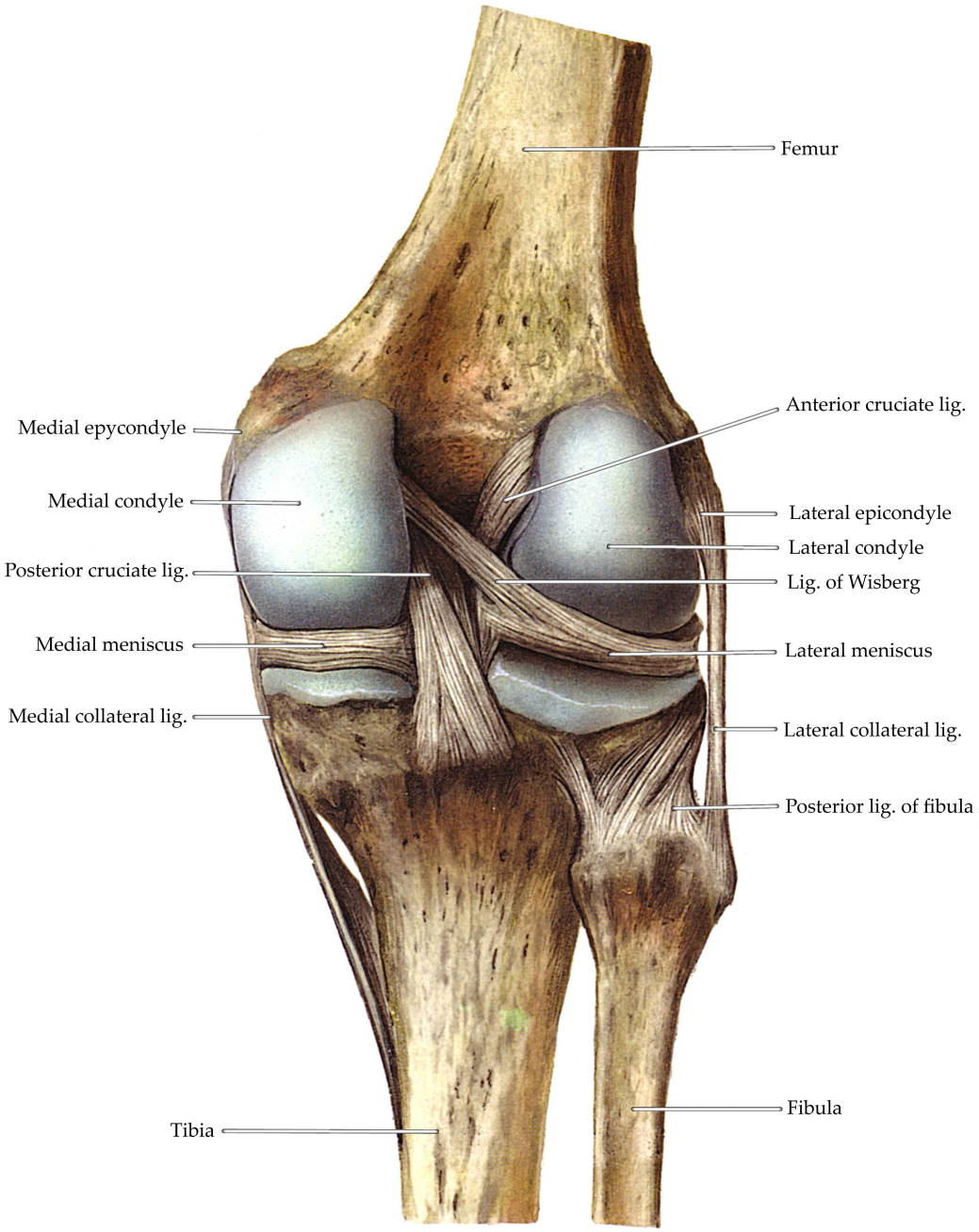

Figure 1.1: *Posterior view of the right knee anatomy [87]*

the superficial medial collateral ligament, the deep medial collateral ligament and the posteromedial capsule [93]. The lateral collateral knee is strawlike in appearance, originates from the lateral femoral condyle and inserts into the posterior proximal fibula. The cruciate ligaments are found in the central part of the knee joint. The ACL originates from the intercondylar notch at the lateral femoral condyle and courses distally

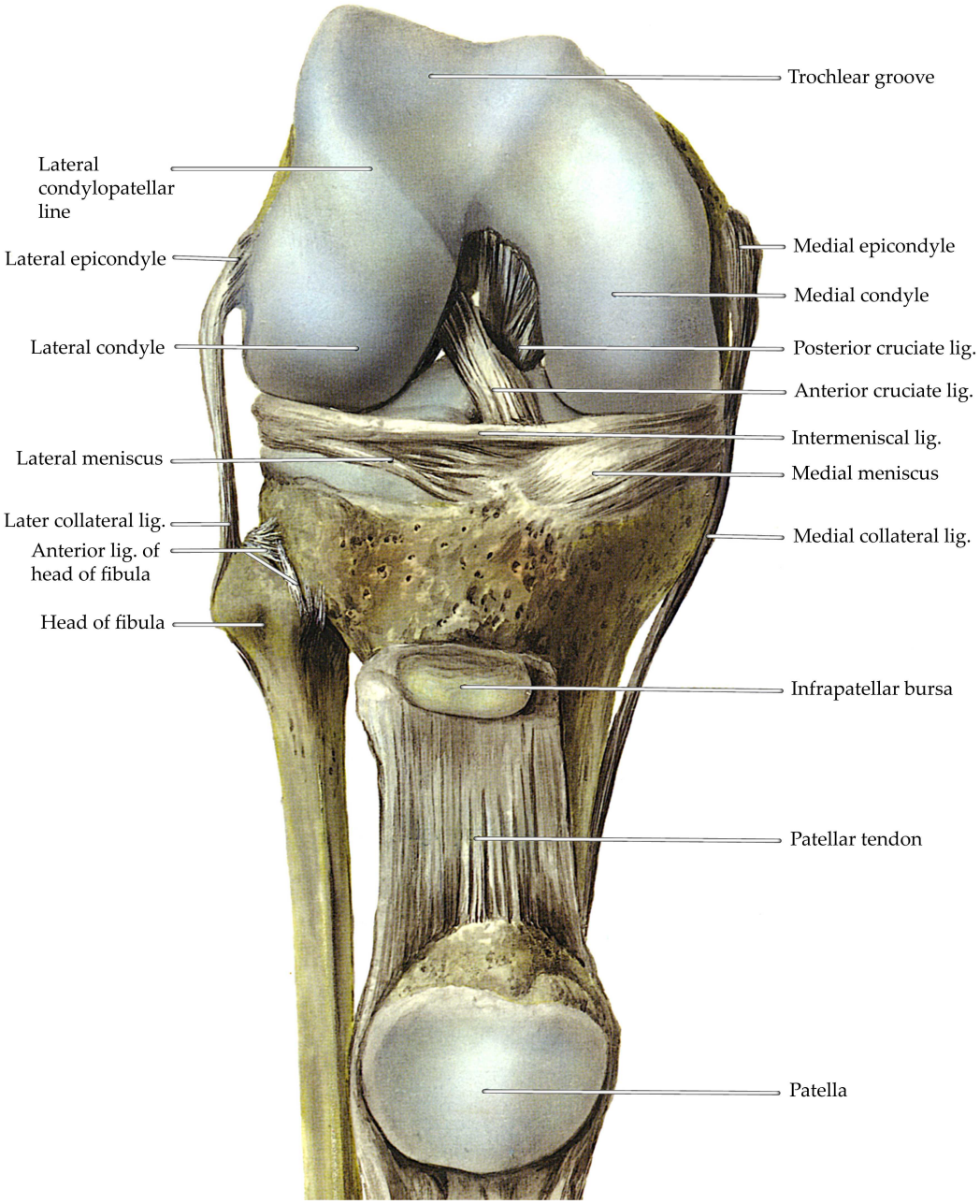

Figure 1.2: *Anterior view of the right knee anatomy [87]*

to the anterior medial tibial plateau. The femoral insertion of the PCL is situated anteriorly on the medial wall of the intercondylar notch. The PCL then proceeds distally to the central posterior surface of the tibial plateau. Both cruciate ligaments are described as consisting of two distinct bundles. This division is based on both the orientation and tensioning patterns of the individual fibers during knee flexion and

extension. Because of their tibial insertions, the ACL is divided into an anterolateral and a posteromedial bundle, whereas the PCL is characterized by a anteromedial and a posterolateral bundle [48, 47, 84].
During flexion of the healthy intact knee, the PCL elongates and tightens, thus exerting a posteriorly directed force that causes the femur to roll back on the tibia [118]. As the center of rotation of the femur and the femorotibial contact points translate posteriorly, the moment arm of the quadriceps muscles increases, providing a mechanical advantage for the muscle in resisting further flexion and in extending the knee [118] and hence determining suitable patellofemoral compressive force [33].

1.1.3 Cartilage and Menisci

The contact area of the articulating bones is coated with avascular porous connective tissue, better known as hyaline cartilage. Its function is to distribute the joint loads over a wide area, decreasing the stresses sustained by the contacting surfaces and thus to allow the relative movement of the opposing joint surfaces with minimal friction and wear[4]. The knee is provided with two menisci: medial and lateral. They consist of fibrous cartilage and exhibit from a transversal view a C-like shape. Their cross section area resembles a wedge that shrinks radially towards the inside of the meniscus. The menisci are placed between the femoral and tibial condyle and sustain the articulation. Because of their wedge-like shape, they act as a support to the incongruent surfaces of the articulating bones reducing the high load stresses acting in the joint.

1.1.4 Muscles

Articulating joints need to be actively driven in order to interact with one another. This mean is provided by skeletal muscles which mainly consist of contractile cells actuated by the central nervous system. Their contractile fibers are usually attached at each extremity to the articulating bone by a tendon. Muscle contraction is divided into three distinct types: concentric, eccentric and isometric contraction. The difference relies on change in length of the fibers during muscle activity: shortening, lengthening and constant length.
The musculature of the knee can be divided into four major areas: the quadriceps, the medial and lateral hamstrings and the posterior gastroc-soleus complex. The quadri-

[4] A coefficient of friction of about $\mu = 10^{-3}$ has been reported [85]

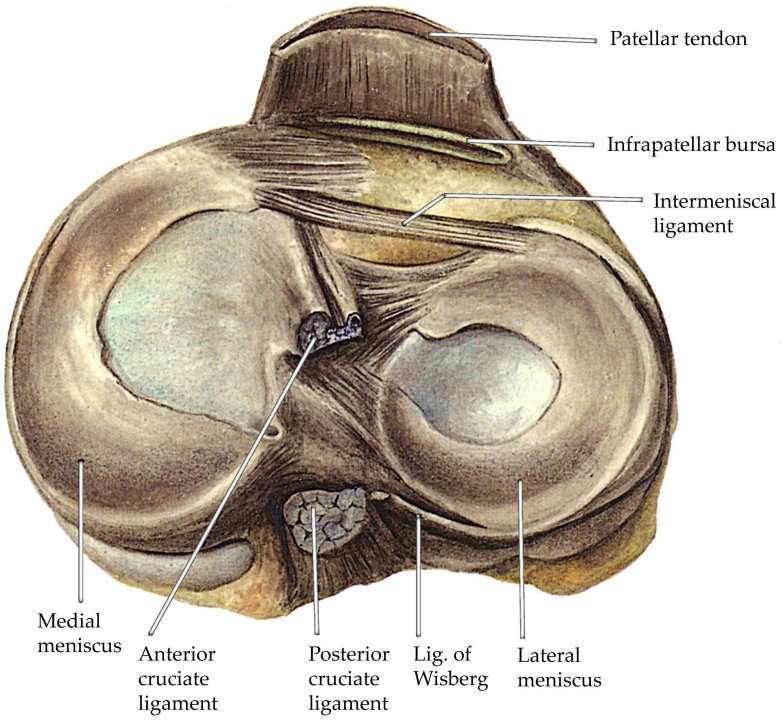

Figure 1.3: *Proximal view of the right tibial plateau [87]*

ceps (rectus femoris, vastii medialis, intermedius and lateralis), which inserts into the tibia through quadriceps tendon, patella and patellar tendon, form the main extensors of the knee.
The medial hamstring (gracilis, semi-membranosus and semi-tendinosus) have origin in the pelvis and insert in the medial side of the tibial metaphysis. They account for flexion and internal rotation. The lateral hamstrings (biceps femoris) originate from the pelvis and the femoral shaft and contribute to flexion and external rotation.
The gastroc-soleus complex includes the gastrocnemius which originates from the posterior femoral condyle and inserts posteriorly into the tuber calcanei. The two heads of the biceps femoris also take part to the flexion of the knee.

1.2 Total Knee Joint Arthroplasty

Nowadays, advanced osteoarthritis in the knee, as in other affected joints, is resolved by replacing the main components of the articulation with an artificial reproduction, which is also referred to as total knee arthroplasty (TKA).

1.2.1 Design Review

The concept of replacing the articular surface of a degenerated joint with soft tissue was already present among surgeons in the middle of the 19th century [114]. In 1861, Ferguson [34] described how to resect an entire knee joint in order to achieve some kind of pseudoarthrosis between the articulating surfaces. Despite the good motion thereby achieved, the results were yet poor because of insufficient stability, and in some cases the joint spontaneously fused.
The first total knee replacement was presented by Gluck in 1890 [50]. He designed a mechanical hinge made of ivory, which was anchored to the bone with cement made of colophony, pumice and plaster of Paris. Despite the fact that it was an outstanding and futuristic concept, this technique showed a high incidence of infection and was quickly abandoned.
In the first half of the 20^{th} century, several attempts were made to resurface the knee articulation with a variety of soft compounds, such as muscular tissue [51], fat and fascia lata [71, 80], skin [12], animal membranes [8], cellophane [96] and nylon [63]. Nonetheless, the achieved results were not satisfactory and to some extent also unpredictable.
In 1940, Campbell [16], assisted by Boyd implanted a Vitallium[5] femoral hemiarthroplasty. Despite the early pain relieve and further development, this type of mold did not become popular because of bad long-term results. Since the exact joint alignment between femur and tibia was difficult to achieve, localized points of high stresses were generated over the articular surface and the implant ended up eroding the preserved cartilage and bone.
The second half of the 20^{th} was very fruitful for the development of total knee replacement. Several different design and surgical procedure were established to improve clinical outcome of reconstructed knees. At first, two distinct type of design philosophy were followed: fullconstrained mechanical hinges and interposition arthroplasty.
In 1958, Walldius reported the results with his hinge design [115]. The prosthesis was made of metal and did not make use of bone cement for fixation. Soft tissue and ligaments were sacrificed. Further adjustments were done by Shier and Young, but their design lacked an articulating surface for the patella. Guepar modified the basic principle of the hinge prosthesis in 1970 by moving the position of the hinge dorsally, which allowed the tibia to rotate under the femur[25]. Furthermore, the extension end stop was damped by means of a Silastic[6] thruster. The implant also accounted for

[5] Vitallium is a term used for an alloy mainly consisting of cobalt, chromium and molybdenum.
[6] A material made of silicone and plastic. Trademark of Dow Corning, Michigan, USA.

a tracking of the patella. Other design followed, e.g. spherocentric knee[7], although nowadays the hinge design is only adopted as a last resort in revision surgery and in widely degenerated knees.
During the 1960s, Gunston drew a new revolutionary type of prosthesis [45]. Accordingly to the anatomy of the human knee, he proposed to substitute the femur condyles with two half circular components, while he designated two articulating polyethylene counterparts for the tibial plateau. Such a design promoted the retention of the main knee ligaments, which helped convey stresses during joint movement. In order to fix the implant, he made use of bone cement. Since the femur runners featured a constant radius over the whole surface, the implant inhibited a physiological flexion of the knee, which resulted in high stresses and eventually caused the implant to fail. Several modification were applied over the next decade, but all showed a consistent failure due to patella pain and loosening.
In 1976 Goodfellow and O'Connor engineered a design with a mobile tibial tray that was supposed to imitate the natural knee kinematics [43]. Because of the high congruency of the femoral component with the polyethylene tray, the implant was very sensitive to alignment errors. A similar design was later implemented in the low contact stress knee mobile bearing prosthesis by Buechel and Pappas [13]. Nowadays, because its revolutionary idea, the concept of a mobile bearing tibial component is adopted in many design.
Charles Townley developed in the early 1970s an anatomic total knee prosthesis, where the trochlea was resurfaced, the cruciates were preserved and bone cement was used for fixation [112]. Thereon, Ranawat, Insall and Walker engineered the Total Condylar Knee, an implant that included the sacrifice of both cruciates and the complete resurfacing of the patellofemoral joint [54]. At the beginning, the prosthesis constituted of a metal femoral component, a polyethylene patella knob and all polyethylene tibial model. Further development introduced new modifications to account for cruciate retaining and for posterior stabilization. Modularity of the tibial component was also achieved by building the bone to implant interface out of metal and combining it with a polyethylene tibial tray. This eventually lead to the numerous designs available today.

[7]The spherocentric knee consisted of a rotating-hinge, where the ball and socket joint lead to triaxial motion.

1.2.2 Cruciate Dependent Design Issues

Since TKA is an artificial reproduction of the human knee, it is obvious that problems are encountered when the preserved parts of the original knee start to interact with the components of the new implanted prothesis. The balance that once was present in the joint is now lost. The question now arises, which parts should be preserved and what are the biomechanical consequences. This inevitably leads to different design philosophies and also to controversies such as the debate whether the retention of the PCL would improve clinical performance and thus life-expectancy of knee replacements or whether the removal of the cruciate ligaments would give better clinical results [50]. This controversy actually relies on the determinant role played by the PCL in human knee joint kinematics and whether the PCL is able to reproduce its function in prosthetic design, as well.

Sustainers of PCL retaining prosthesis argue that PCL retention desings promote more natural kinematics and maintain the proprioception and load transfer capabilities of the ligament [118]. Worland et al. [117] describe that retention of the PCL prevents dislocation of the knee, which may occur in a PCL-substituting knee when the flexion and extension gaps are not carefully balanced. In addition, Andriacchi et al. [5, 6] point out that shear forces are transmitted through the intact PCL, which lowers the shear forces at the fixation interfaces and articulating surfaces, thereby reducing polyethylene stresses. Further studies show that excellent clinical results and range of motion can be achieved with the use of recession to balance the PCL in conjunction with more conforming polyethylene inserts [7, 19, 92, 98, 117].

However, several reports based on fluoroscopic analysis demonstrated that both PCL retaining and PCL substituting designs fail to reproduce normal femoral rollback during flexion [9, 27, 109]. Moreover, believes that proper proprioception would be maintained in total knee replacement through the PCL retention are yet to be confirmed. Studies comparing cruciate retaining with cruciate substituting designs with regard to proprioception could not assess a significant difference between the two TKA approaches [102, 116]. As regard to anteroposterior stability provided by the intact PCL, advocates of cruciate substitution design argue that the functionality of the posterior cruciate ligament needs to be restored during surgery, if necessary by release. Though, this presents a major technical challenge [50] because of the difficulty in balancing the ligaments with the replacement joint morphology. Numerous reports show that a improper balanced PCL can result in TKA instability during either flexion or extension, and in some severe cases a overly tightened PCL has been shown to tear [26, 67, 76, 82].

Up to now, the cruciate controversy is yet to be elucidated. As shown in table 1.1,

several studies about the survivorship of posterior cruciate retaining and posterior stabilized TKA designs do not succeed to draw a clear and satisfactory line between the two approaches. Nonetheless, this unequivocally shows that a considerable number of subjects still have to deal with a failed knee replacement, and therefore, further investigations are inevitable.
As argued above, scientist still seek after a clear and founded explanation why one design will perform better than the other, or even why there are no relevant discrepancy with regard to patient outcome. There still are some aspects of the knee biomechanics that eventually need to be further clarified. This argument applies to healthy, deficient and reconstructed knee joints. To a certain extent, it could seem like the existing measuring methods either do not provide the representative data or are not yet suitable to be used in crucial situation, where relevant information is expected, e.g. stair descent over several steps. In this case, a more accurate or an improvement of the existing methods can substantially assist scientists in promoting new findings in knee biomechanics.

1.3 Biomechanical Assessment of the Knee Joint

Although the anatomy of the knee joint is very well defined and understood, as described in section 1.1, its mechanical function and properties are still of great interest

Study	**No. knees**	**Survivorship (%)** at 10 years
Cruciate retaining TKA		
Schai et al. [97]	235	90
Berger et al. [11]	109	100
Gill and Joshi [42]	404	98.2
Buechel et al. [14]	373	98.3
Sextro et al. [100]	168	96.5
Posterior stabilized TKA		
Colizza et al. [22]	101	96.4 at 11 years
Ranawat et al. [86]	125	97 at 6 years
Stern et al. [108]	194	94 at 13 years
Scuderi et al. [99]	917	98.75 at 7 years

Table 1.1: *Studies about the survivorship of total knee arthroplasties*

to the biomechanical research community, because of its high level of complexity. Furthermore, a profound knowledge of the mechanics acting on the knee joint is essential for the description and the understanding of knee deficiencies, which has a great impact on treatments and preventions of knee degenerating diseases.
In order to study and analyze the functionality of the human knee complex, the scientists rely on different types of measuring systems and mathematical procedures, such as movement analysis and mechanical descriptive models of the knee.

In biomechanical gait analysis, external skin mounted markers in conjunction with force measurements have been extensively used to specify the mechanical in vivo behavior of the knee. The idea behind this approach is to represent the position and orientation of the bones by the 3D-coordinates of the marker clusters derived by video-photogrammetry. Ground reaction forces (GRF) are simultaneously acquired by means of force plates.
Based on inverse dynamics, which implies the definition and the formulation of a *well posed* joint model, the net-forces and net-moments acting in the joint can be directly obtained. Unfortunately, due to soft tissue artifacts, the skin is not firmly fixed to the underlying bones, i.e. the skin mounted markers attached to the shank and the thigh show slightly different trajectories than the one carried out by the actual bones [89, 90, 106]. Therefore, if the kinematics of the knee joint were promptly derived from the external markers without any further processing, a significant error would be introduced, which would further lead to inaccurate statements about the joint complex. In the past years, several methods have been developed to overcome soft tissue artifacts and to accurately determine the six degree of freedom kinematics of the underlying bones using external skin markers. Although the effect of the soft tissues interposed between the markers and the underlying bones can theoretically be modeled by means of the Interval Deformation Technique [1, 2, 106], soft tissue artifacts is still strongly dependent on the kind of activity and on the individual subject. Thus, the pose estimation of the bones in video-photogrammetry based human motion analysis is still very critical [18, 20, 23, 68, 106, 70].
An other approach to determine bone position during several activities is based on bone pins, external reflective markers fixed on intracortical pins, that are directly screwed into the bone structure [64, 65, 66]. This method was also used to study skin markers behavior [89, 90]. Although intracortical pins are a very accurate tool to assess the kinematics of the human underlying structure, their usage is limited to a restricted number of subjects due to the invasive procedure and set up.
In the past decade, a great effort has been put into assessing the kinematics of the knee joint by means of video fluoroscopy. This system returns a contiguous series of X-ray

images of the joint taken at a specified sampling frequency. The three dimensional information of the knee gathered by magnetic resonance imaging (MRI) or computed tomography (CT) scanning can further be matched onto the images retrieved by the video fluoroscope through a dedicated algorithm. This is a promising method to provide a good insight of the knee kinematics [28, 29, 59, 72, 73, 74]. A remarkable drawback of this technique is the limited field of view of the video fluoroscope: the measuring equipment is normally static, while the knee repeatedly changes its position and velocity in space. In other words, it is merely possible to retrieve scientifically useful images of the knee joint during a small part of the gait cycle, which is clearly not enough for a complete biomechanical analysis of human movement. For instance, Fantozzi et al. [32] were able to examine a mobile bearing PCL retaining vs. a posterior stabilized TKA during stair ascent for relatively small people only [8], because the range of motion of the knee during such an activity is small enough to fit into the field of the fluoroscopic imaging unit.

At first sight, a solution could be to perform fluoroscopy based gait analysis on a treadmill. Doing so, two salient problems arise: 1. the gait pattern is altered compared to the undisturbed situation [81, 110], 2. retrieval of kinematics information for a full gait cycle becomes unfeasible due to the constrained imaging field.

At the Institute for Biomechanics of the ETH in Zurich, an automated moving video fluoroscope was developed to steadily track the knee of a subject over several steps of level walking (figure 1.4). Once the method to retrieve the six degree-of-freedom kinematics of the femorotibial joint has been assessed, the procedure can be combined with a ground reaction force measuring system, thus enabling an extended analysis of the mechanics of the knee during several full gait cycles. Zihlmann et al. [123] were the first to gather combined fluoroscopic and force data for unconstrained level walking. This study gave a clear perception of the amount of sensitive data such a measuring set up can deliver and showed the way for a very promising approach in the field of biomechanics.

New and innovative measuring equipment for movement analysis are important because of the improved and more reliable insight and data they provide. Nevertheless, it is even more crucial to identify and analyze those motion activities that provoke discomfort to subjects with knee deficiencies. Consequently, further and focussed development can be achieved in knee rehabilitation and knee prevention.

In the biomechanical community, it is well accepted that stair motion activities are one of principle causes of a suffering condition for most of the subjects with knee disorders [21, 79, 78, 91, 94, 120, 121]. Stair activities can be stressful and cause in-

[8] Average height were 161cm and 157cm for the first and the second group respectively.

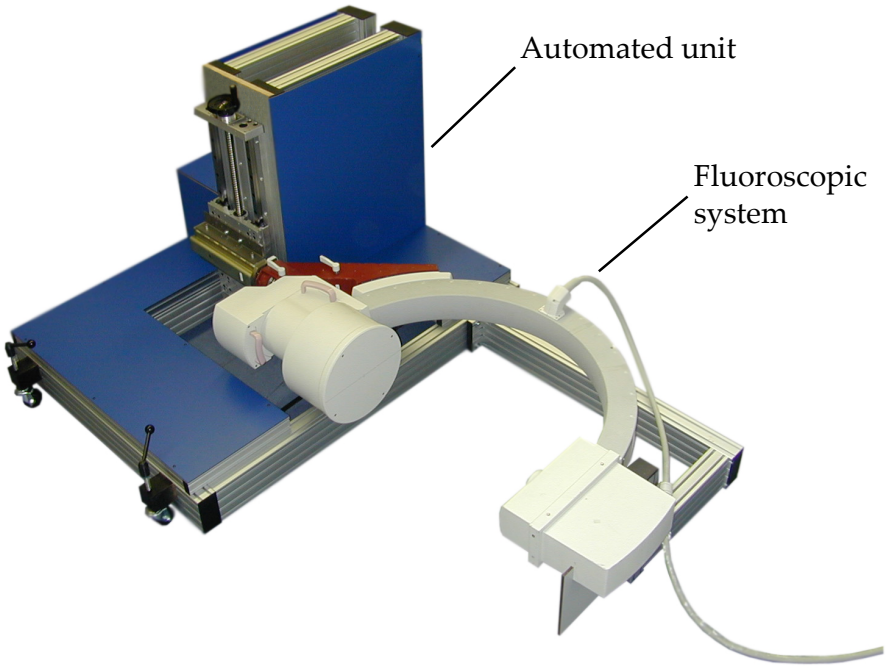

Figure 1.4: *The above automated fluoroscopic system was developed for the* in vivo *investigation of human level gait.*

juries that can end in death [35, 21]. It is also considered to be the less stable gait pattern and to best reproduce pathological symptoms [95, 104]. Because of the higher demand on muscle force and thus higher lower-limb moment production than other daily activities [60, 57, 77, 83, 103], subjects affected by knee disorders often develop compensatory movement to safely complete the task [56, 95]. Therefore, analyzing stair descent clearly adds to the understanding of pathological motion patterns and represents one of the most relevant activity to study the mechanics of knee disorders. Thereby, it is imperative that a thorough biomechanical analysis is performed with more accurate measuring systems, than it has been done so far.

1.4 Aim of this Dissertation

The big variety of knee prosthesis designs available on the market today is a sign of advanced technical progress. However, a consistent number of subjects still exhibit serious difficulties after total knee replacement. Furthermore, as survivorship studies apparently show, the success of the clinical outcome is not necessarily or exclusively dependent on the type of arthroplasty design that the market offers so far (table 1.1). Consequently, in order to assess the best surgical procedure and the optimal arthroplasty design and thus improve clinical outcome, deeper insight into the in vivo mechanics acting on the knee joint and implant components is needed. Moreover, it is also imperative to gather relevant and accurate information during those activities where the patients register the biggest discomfort, such as stair descent (section 1.3). Therefore, the aim of this dissertation is the

> *In vivo measurement of the kinematics and kinetics of total knee replacement during unconstrained stair descent*

For this purpose, the following subordinate targets become inevitable:

- The existing fluoroscopic based gait analysis has to be improved in order to gather more accurate kinematic and kinetic data of the knee joint during stair descent than it is currently possible. Therefore the following objectives need to be reached:
  - Upgrade of the horizontal and addition of the vertical displacement to the automated fluoroscopic equipment
  - Enhancement of the quality of fluoroscopic images and the subsequent image processing chain
  - Design of a new instrumented stair case
  - Correction of the orientation of the force that relies on force plate measurements
- Comparison of video-photogrammetry with video-fluoroscopy based stair descent analysis with respect to total knee joint replacement kinematics and kinetics

Scientists investigate that which already is;
Engineers create that which has never been.

Albert Einstein (1879 - 1955)

2 Methods

The following sections describe the experimental set up developed and employed for the acquisition of the mechanical data for this work. Kinematics were gathered by means of an X-ray imaging system and a video photogrammetry based positioning system, whereas kinetic data were collected through piezoelectric force plates.

2.1 Video Photogrammetry

Video photogrammetry is extensively used in the field of biomechanics for motion analysis purposes (section 1.3). The principle of video photogrammetry is to reconstruct the three dimensional coordinates of a point from the two dimensional views of synchronized cameras. Using projective geometry, the rays originating from each camera center passing through the recorded projection of the tracked point are extended into space. The 3D point coordinates are then given by the intersection point of the rays originating from the cameras.
Theoretically, two synchronous independent projections of the object suffices to provide a system of three linear equation for the three unknown variables. Nonetheless, this assumes that no source noise is present in the system. With other words, this means that the intrinsic and extrinsic camera parameters are exactly defined and time invariant and that the 2D coordinates of the camera view can be determined infinitesimally. In real applications, this is never the case. Therefore, motion capture systems, which are nowadays available on the market, introduce redundant information by

applying a large number of cameras. This provides an overdetermined system of equations, which can easily be solved using an appropriate optimization procedure.
The Institute for Biomechanics (IfB) of the ETH Zurich is equipped with a Vicon MX (Oxford Metrics Group, UK) motion capture system. It features eight fixed in place and four mobile F40 cameras. Each camera is equipped with an infrared stroboscope (figure 2.1). The built in charge-coupled device (CCD) sensor accommodates a matrix of 2352×1728 pixel and has a maximal capture rate of $370\,^{\text{frame}}/_{\text{s}}$. Each lens accommodates an infrared filter, so that each camera mainly registers those object that best reflect the light emitted by the connected stroboscope. Therefore, the markers that need to be tracked are coated with a high reflective material (figure 2.2).
At system start up, the user needs to calibrate the motion capture system, i.e. the intrinsic and extrinsic camera parameters need to be assessed. By means of a beam with 3 reflective markers mounted at well defined positions, the user scans the whole capturing volume, so that the system has enough data for a stable optimization of each parameter.
During motion capture, each camera automatically evaluates the position of the sensed markers in its projective plane. The two dimensional coordinates are then sent by each camera to the main software, which, after proper world calibration, directly computes the 3D world coordinates of each marker. For a measuring volume of the size used for gait analysis, the marker position can be assessed with a root mean squared error $\sigma_{\text{Vicon}} \leq 1\,\text{mm}$.

2.2 Video Fluoroscopy

Video fluoroscopy is a technique used in clinical environment in order to capture a continuous series of real time X-rays images of a part of the body that can be viewed on a monitor screen.

Figure 2.1: *Vicon MX F40 camera* `www.vicon.com`

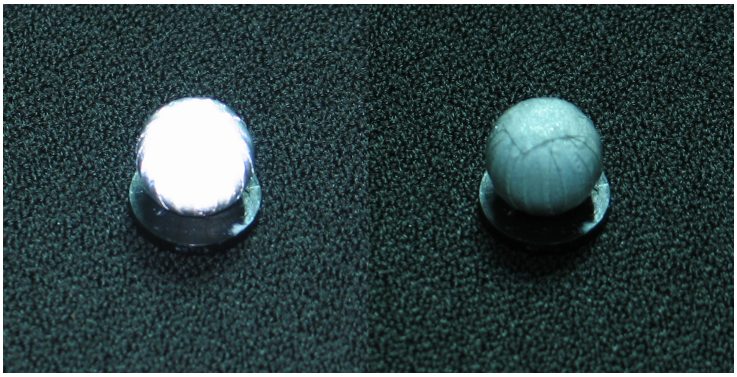

Figure 2.2: *On the left a reflective marker illuminated by a light source positioned at the observer location. On the right the same marker illuminated by a light source out of the line of sight.*

2.2.1 Image Acquisition

The X-ray source and detector of the fluoroscopic unit are aligned together by a C-shaped arm that keeps the detector in the line of sight of the high energy photons at all time. The X-ray source is connected to a generator, which provides the energy to accelerate the electrons towards the rotating anode in order to develop a X-ray cone beam. The detector, in the present system set up also known as image intensifier, converts the energy of the X-ray photons into visible light (figure 2.3). The video fluoroscope used for the kinematic data collection in this work corresponds to a complete fluoroscopic medical system operating at clinical standards (BV Pulsera, Philips Medical Systems, Switzerland. Figure 2.4). The image intensifier has a diameter of 12 inches and contains a CCD camera with 752×582 effective pixels. The storage matrix adds up to 768×576 pixel with a grayscale resolution of 8 bit. The system allows to record X-ray videos at a sampling rate of up to 25 $^{\text{frame}}/_{\text{s}}$ with a shutter period of 8 ms. The video generation is achieved by a pulsating X-ray beam. Therefore, the patient exposure is constraint to a minimum.
Since the build-in camera is not accessible for modifications and tuning of the image acquisition, a new stand alone CCD detector was incorporated into the fluoroscope. Thus, it is now possible to directly access the digital information collected by the CCD sensor prior to any further processing and to also tune the acquisition parameters such as shutter period, beginning of integration and intensity gain. By decreasing the default image integration time down to 1 ms, as adopted in this study, and thus reducing the artifacts due to motion blur, a sharper image of the moving implant is achieved. Furthermore, the storage matrix of new CCD sensor amounts to 1000×1000 pixel with a grayscale resolution of 12 bit, which enhances the overall quality of the image. The

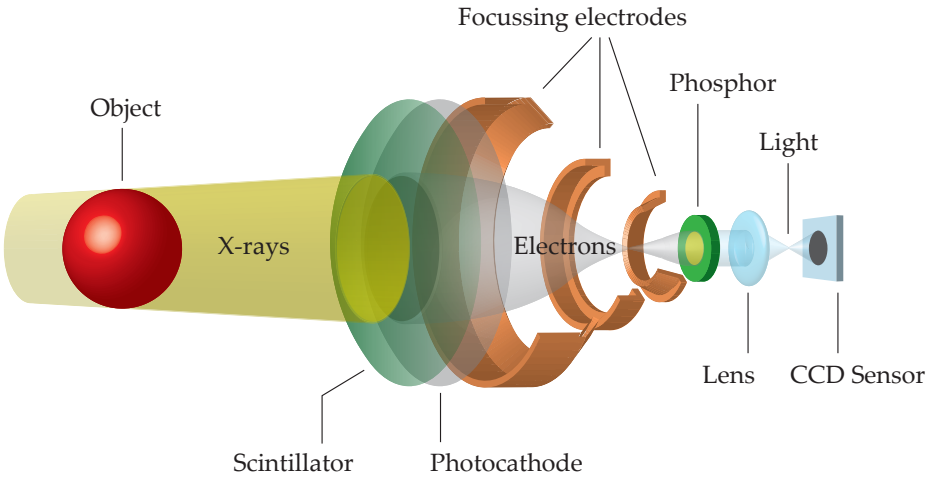

Figure 2.3: *Image Intensifier: At first, the ionizing photons generated by the X-ray source strike on the desired object. The outcoming photons which were not totally absorbed interact with the input phosphor screen, also known as scintillator. This, in response, fluoresces photons at a lower energy. The subsequent, hereby excited, photocathode emits photo electrons in direction of the anode. While being accelerated towards the anode, the electrons are focussed towards the output phosphor by means of particularly arranged electrostatic lenses. The lastly emitted photons possess a visible light spectrum and, thereby, can be easily detected through a video capture device.*

default imaging system generates an image where a maximum of 0.7 lp/mm[1] can be distinguished. In the radiographs created with the new CCD sensor, the maximal resolution is of 1.6 lp/mm (figure 2.5).
In order to synchronize the video photogrammetry system and force measurements with the X-ray imaging chain, the fluoroscopic equipment is connected to the Vicon acquisition system. The input trigger sent by the X-ray generator to the CCD sensor is wired to an analog input of the gait analysis equipment. Hence, the exact time of the radiographic exposure is constantly recorded.

2.2.2 Image Distortion Correction

If a well defined reference grid is placed perpendicularly to the X-ray beam of the fluoroscope, the resulting exposure will exhibit a disrupted projection of the original geometry (figure 2.6a).
The geometric image deformation caused by the fluoroscopic imaging chain can be

[1] lp/mm = line pairs pro millimeter

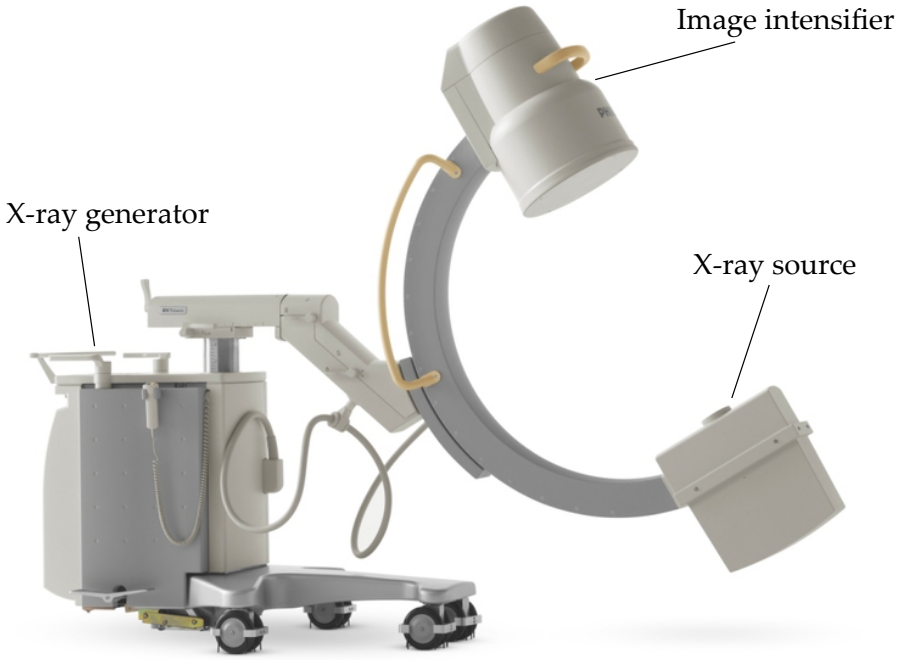

Figure 2.4: *Philips BV Pulsera clinical fluoroscopic system*

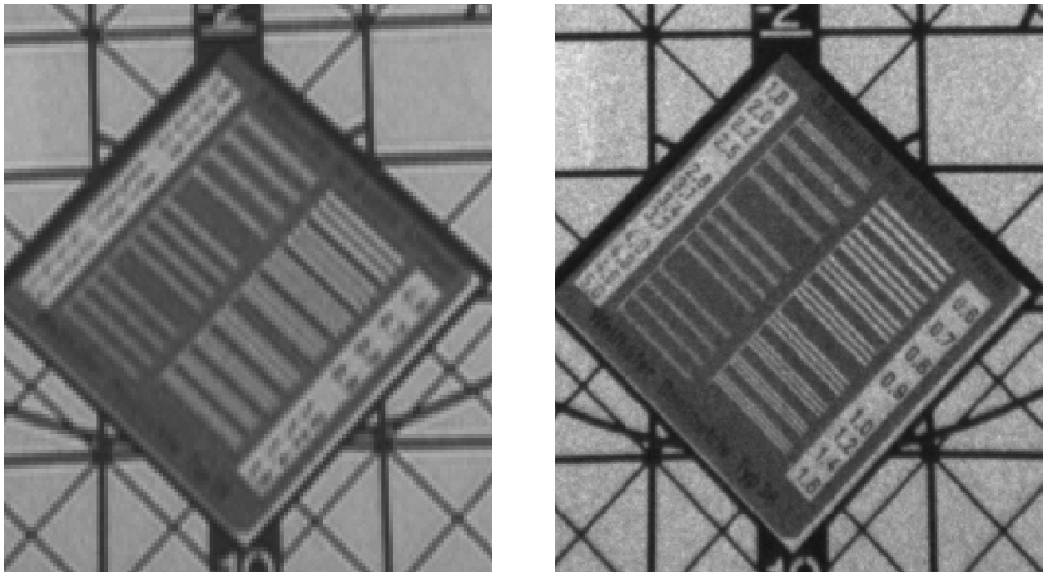

(a) Old CCD (b) New CCD

Figure 2.5: *The pictures above show two X-ray images of a calibration plate, taken with the standard built-in camera (left image) and with the new CCD detector (right image). The optical resolution in the first case is about 0.7 lp/mm, in the second 1.6 lp/mm.*

divided into radial and sigmoidal distortion. In the first case, the convexity of the input phosphor screen and photocathode combined with the lens objective placed in front of the recording CCD camera produces a radially distributed variation and magnification of the incoming projection. Sigmoidal image distortion, on the other hand, is induced by the interaction of the external magnetic field with the internal electron beam, that is accelerated toward the output phosphor.
Since the relative position of the beads to one another is known, the projection of the reference grid can be restored by means of a polynomial approximation. The acquired image is divided in adjacent quadrilateral regions defining the bead as their vertices. Then, a first order polynomial is solved over each region [9]:

$$\mathbf{u} = a_0 + a_1\mathbf{x} + a_2\mathbf{y} + a_3\mathbf{xy}, \tag{2.1}$$

$$\mathbf{v} = b_0 + b_1\mathbf{x} + b_2\mathbf{y} + b_3\mathbf{xy} \tag{2.2}$$

in matrix form

$$\begin{pmatrix} u_0 \\ u_1 \\ u_2 \\ u_3 \end{pmatrix} = \begin{bmatrix} 1 & x_0 & y_0 & x_0y_0 \\ 1 & x_1 & y_1 & x_1y_1 \\ 1 & x_2 & y_2 & x_2y_2 \\ 1 & x_3 & y_3 & x_3y_3 \end{bmatrix} \begin{pmatrix} a_0 \\ a_1 \\ a_2 \\ a_3 \end{pmatrix}, \qquad \begin{pmatrix} v_0 \\ v_1 \\ v_2 \\ v_3 \end{pmatrix} = \begin{bmatrix} 1 & x_0 & y_0 & x_0y_0 \\ 1 & x_1 & y_1 & x_1y_1 \\ 1 & x_2 & y_2 & x_2y_2 \\ 1 & x_3 & y_3 & x_3y_3 \end{bmatrix} \begin{pmatrix} b_0 \\ b_1 \\ b_2 \\ b_3 \end{pmatrix}$$

where $\mathbf{u} = (u_0, u_1, u_2, u_3)^t$ and $\mathbf{v} = (v_0, v_1, v_2, v_3)^t$ are the horizontal and vertical coordinates of the four centroid of the beads forming a quadrilateral region in the image plane, $\mathbf{x} = (x_0, x_1, x_2, x_3)^t$ and $\mathbf{y} = (y_0, y_1, y_2, y_3)^t$ are the correspondent known coordinates in the grid frame. a_0,...,a_3, b_0,...,b_3 are the unknown distortion coefficients.
Once the coefficients $a_{0\cdots3}$ and $b_{0\cdots3}$ are extracted for each region, the coordinates $[u_i, v_i]$ plane for every pixel i in the output undistorted projection are calculated. Since the resulting coordinates do not fit the discrete pixel grid of the distorted input image, the gray level intensity of the output pixels is computed by bilinear interpolation of the neighboring input pixels (figure 2.6b). In order to quantify the error introduced by the distortion correction, the reference grid was rotated arbitrarily in the image plane. The recorded X-ray exposure was further corrected with the previous calculated correction parameters. The centroid of each bead was computationally determined for the entire image. The relative rotation and translation of the grid was obtained by means of a least square optimization over the found centroids and the known coordinates of the beads in the grid reference frame. The resulting deviation of the centroids in horizontal (x-axis) and vertical (y-axis) direction is depicted in figure 2.7 by means of intensity plots. With a root mean squared error (RMSE) of $\sigma = 0.03\,\text{mm}$, the error accounts to $\varepsilon = 0 \pm 0.03\,\text{mm}$ for both axis x and y.

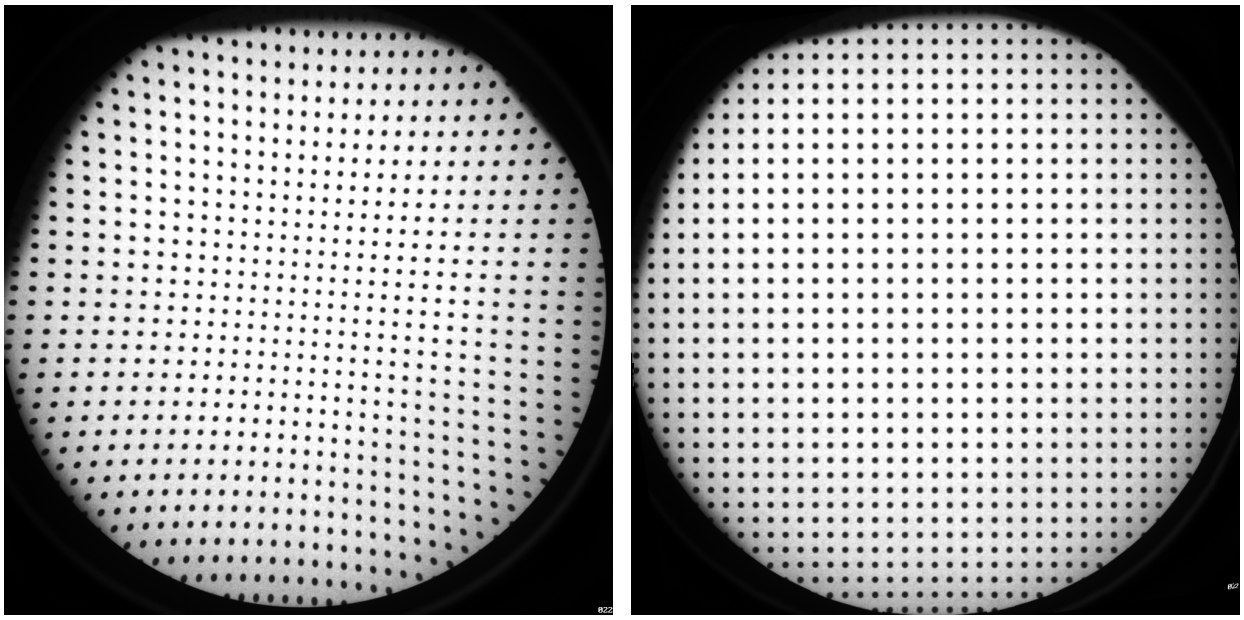

(a) Distorted X-ray image (b) Image after correction

Figure 2.6: *X-ray image distortion correction: On the left, the distortions introduced by the image intensifier to the reference grid are clearly visible. On the right the same image after image distortion correction.*

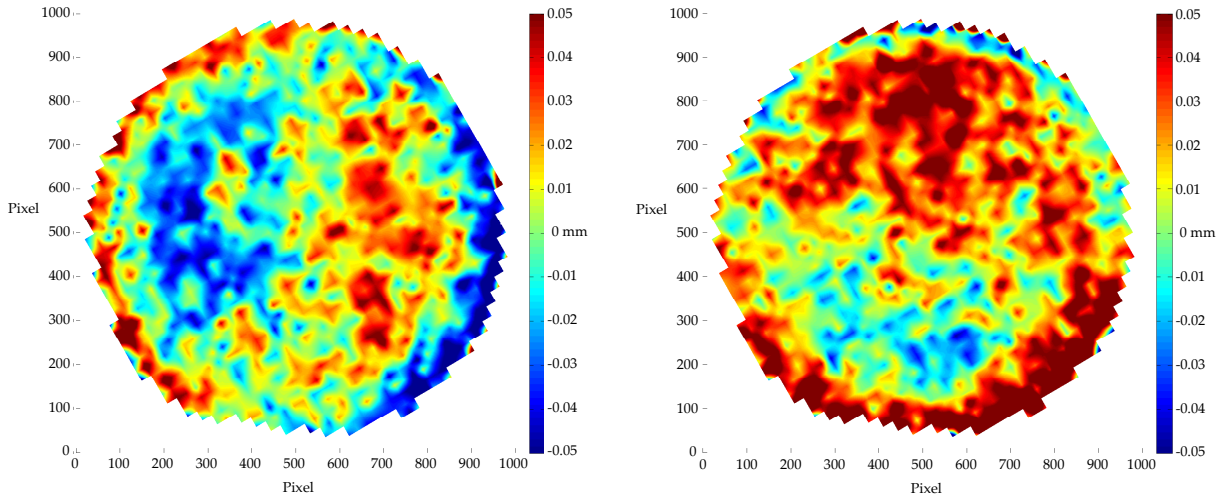

(a) Horizontal error (b) Vertical error

Figure 2.7: *Error after distortion correction: The images show the intensity plot of the error in horizontal and vertical direction after image distortion correction. The values on the color bar are specified in millimeters.*

2.2.3 Projection Geometry

In section 1.3, it is anticipated that the kinematics of well defined objects can be retrieved from a series of two dimensional fluoroscopic images by means of a dedicated reconstruction algorithm.
In order to properly recover the position of the tracked object relative to the fluoroscopic system, the projective geometry involved in image formation has to be known. X-ray imaging can be described by means of a basic pinhole camera model, where the image formation is described as the central projection of three dimensional points in space from a defined camera center **C** onto a two dimensional plane. By defining **C** as the origin of the Euclidean $\mathbb{R}^3$ coordinate space and letting $Z = f$ describe the image plane, the projection is defined as the following correspondence:

$$(X, Y, Z)^t \longmapsto (f\tfrac{X}{Z}, f\tfrac{Y}{Z})^t.$$

By means of homogeneous coordinates, the central projection is simply expressed as a linear mapping [49]:

$$\begin{pmatrix} X \\ Y \\ Z \\ 1 \end{pmatrix} \longmapsto \begin{pmatrix} fX \\ fY \\ Z \end{pmatrix} = \begin{bmatrix} f & & & 0 \\ & f & & 0 \\ & & 1 & 0 \end{bmatrix} \begin{pmatrix} X \\ Y \\ Z \\ 1 \end{pmatrix} \tag{2.3}$$

$$\mathbf{x} = \mathsf{P}\mathbf{X} \tag{2.4}$$

Taking the translation and the rotation of the camera system into account, the projective transformation P is now described as

$$\mathsf{P} = \mathsf{K}[\mathsf{R} \mid \mathbf{t}], \tag{2.5}$$

where R is a 3×3 rotation matrix, $\mathbf{t}$ a three dimensional displacement vector and K is defined as follows

$$\mathsf{K} = \begin{bmatrix} m_x f & s & x_0 \\ & m_y f & y_0 \\ & & 1 \end{bmatrix}$$

Here, m_x and m_y account for scale factors of the CCD sensor matrix in the case of non-square pixels, s represents the skew of non-perpendicular arrangement of the sensor columns and rows. $(x_0, y_0)^t$ are the coordinates of the principal point in image plane coordinate system. In this case $m_x = m_y = 1$ and $s = 0$.
It can be seen from equation 2.5 that, in order to asses the camera matrix P of the fluoroscopy system, at least 6 point correspondences are needed. Since the X-ray image

generation is affected by acquisition noise, redundancy has to be added to the system in order to provide a better approximation of the unknown parameters. For the latter purpose, a reference calibration grid was designed. It consists of a 300 mm long tube and two plates made of Plexiglas® (figure 2.8). At well defined positions (accuracy: ± 0.03 mm), each plate was filled with 12 and 13 metal pellets respectively. This gives a total of 25 point correspondences, which were used to compute the camera matrix P by a least squares optimization.

Once the projection geometry parameters of the fluoroscopy equipment are assessed, its orientation and location relative to the video-photogrammetric system can be calculated. For this purpose, the grid used for image distortion correction is equipped with six reflective markers screwed at predefined positions. The grid is then rotated and displaced, while radiographs of the grid's beads and photographs of the markers are simultaneously taken. This gives a series of correspondences of the grid X-ray projections and three dimensional orientations and locations of the pellets. Since the projection matrix K is now determined, equation 2.5 is used in the least squares optimization to compute $[\mathsf{R} \mid \mathbf{t}]$, which defines the orientation and position of the fluoroscopy system relative to the video-photogrammetric equipment.

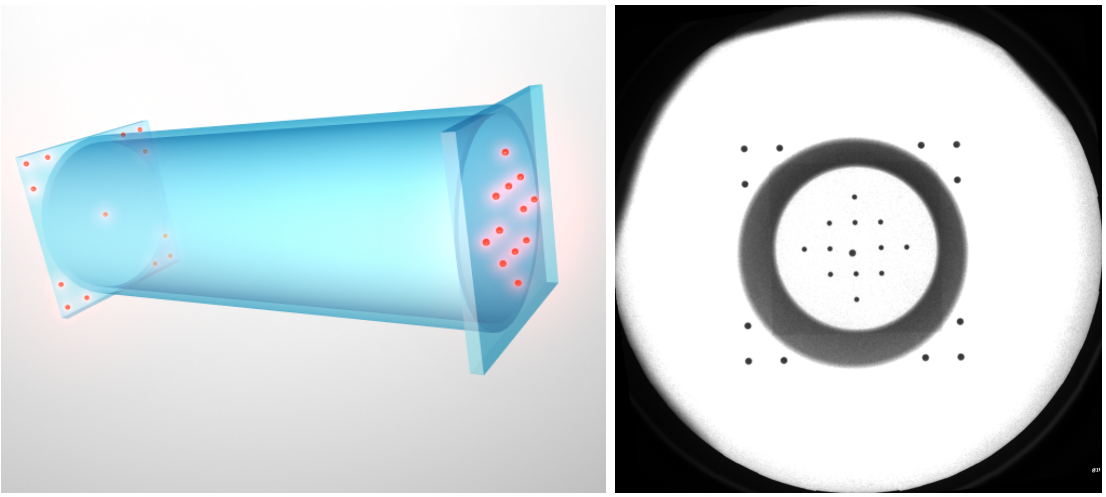

Figure 2.8: *On the left a 3-dimensional model of the construct used for camera parameter estimation. In the body (blue), which is made of Plexiglas®, 25 steel beads (red) were planted at a predefined position. The right picture shows an X-ray shot of the construct.*

2.2.4 2D-to-3D Registration

X-ray images are substantially two dimensional projections of three dimensional objects. Assuming that an exposed target is not rotationally symmetric, it is feasible to reconstruct its orientation and position in space out of the two dimensional X-ray image. The idea behind this is to first compute a digital-reconstructed radiograph (DRR) out of the volume information of the object, and then, by means of an optimization algorithm, to locate its relative pose in space by sequentially comparing the DRR with the actual X-ray fluoroscopic image [15].
For present work, the registration algorithm developed in [15] was embedded in a new graphical user interface in order to ease the user interaction and increase the workflow by make it more intuitive. The software allows to navigate three dimensionally around the pose estimation computed by the registration algorithm in order to asses any anomalies after registration. Furthermore, the overall performance of the original algorithm has improved by decreasing the computing time from a couple of minutes to less than one minute for the same image and object constellation.

Registration error

For a reliable biomechanical analysis of the human knee, it is necessary that the position of the joint components are obtained as accurately as possible. Therefore, the error induced by the registration algorithm needs to be quantified.
Although the performance of the algorithm used in this study has been previously investigated [123], the subsequent improvements made in the imaging chain, such as camera resolution and distortion correction enhancements, required a new error assessment for the reconstruction procedure.
In order to evaluate the reconstruction results, the prosthesis components were adjusted at predefined locations by means of a positioning setup. This comprised an industrial cross table (0.01 mm) and a marking unit (0.1 mm), which were screwed to one another to build a three dimensional positioning system (figure 2.9). The prothesis components were first fixed together and embedded in a polyurethane foam to prevent any relative movement against each other. Consecutively, they were fastened to the marking unit.
A total of 63 X-ray images of the prosthesis were taken at different coordinates, thus providing a valuable amount of information for error assessment. The protocol positions are schematically given in figure 2.10. Since the coordinate system of the cross table and the one of the registration algorithm are not coincident, the Euclidean trans-

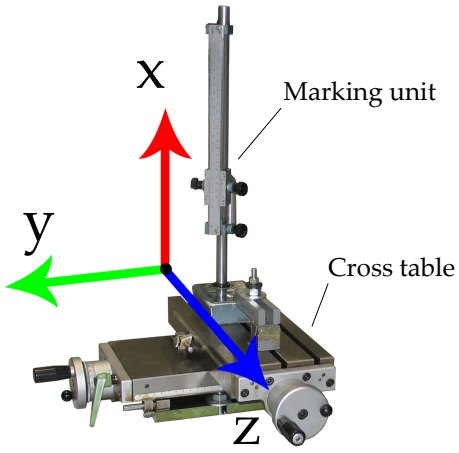

Figure 2.9: *Positioning setup for error evaluation*

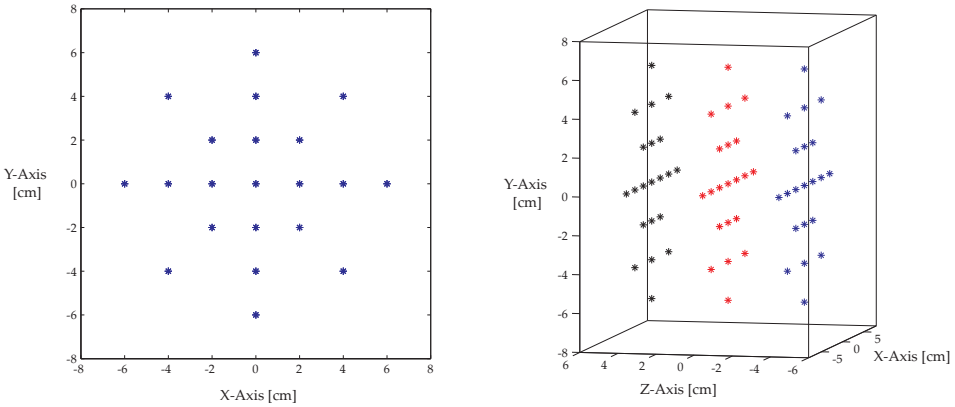

Figure 2.10: *Positioning of the prosthesis for error estimation of reconstruction algorithm. The X and Y axis are parallel to the imaging plane, while the Z axis is collinear to the focal line.*

formation that relate them to each other has to be computed. Assuming the algorithm does not induce any rotational and translational bias, the coordinate transformation $\mathsf{H} = [\mathsf{R} \mid \mathbf{t}]$ is given as follows

$$\mathsf{H} = \underset{\mathsf{H}}{\operatorname{argmin}} \sum_{i=1}^{N} (\tilde{\mathbf{x}}_i - \mathsf{H}\mathbf{x}_i)^2 \tag{2.6}$$

where $\mathbf{x}$ are the homogeneous coordinates of the position of the prosthesis in the cross table coordinate system and $\tilde{\mathbf{x}}_i$ are their mappings given by the registration algorithm. After applying the coordinate transformation H to the results of the registration algorithm, the root mean squared error of system is calculated (table 2.1).

At this point, it is important to note that for this error assessment the digitized volumetric data of the prothesis was employed. Thus, the implant underwent a three dimensional scanning procedure[2].
Unfortunately, the exact volumetric data of the prosthesis components is not available during the evaluation of in vivo experiments. The only possible way to retrieve the implant data would be to digitize the surface prior to implantation. This procedure was not applied for the subjects analyzed during this project. Instead, the CAD data was used to determine the position of the implant components. Hence, the manufacturing accuracy of the prosthesis had to be determined.
The deviation of the true volume to the design and construction drawings of the femoral component is visualized in figure 2.11. It can be noticed, that the discrepancy of the surface is at its minimum at the bearing surface of the condyles, while the biggest difference is found at the edges of the implant. Appreciably, the latter structural part is where the accuracy and the precision of the final construction are not relevant for the articulation of the implant components and thus does not negatively affect the overall functionality of the prosthesis. However, this incongruity has a distinct impact on the registration results.
The following example illustrates the effect of this source of error. It is well accepted, that X-ray image formation of macroscopic object can be described with basic projection geometry, thus assuming that the X-ray cone beam acts as a pinhole camera. In this study, the average object-to-focus distance is about 900.0 mm and the size of a knee prosthesis approximately 60.0 mm. If an object of half the size of a knee im-

[2]The principle behind this type of measurement is to project different predefined patterns on a surface while a highly sensitive camera captures the several projections. By means of a dedicated algorithm, it is subsequently possible to reconstruct the selected volume out of the several distortions of the projected patterns. For more information please see: optoTOP-HE, Breuckmann, www.breuckmann.com.

		Femoral component	*Tibial component*
Translation σ [mm]	X	0.24	0.28
	Y	0.12	0.22
	Z	0.80	1.02
Rotation σ [°]	X	0.19	0.13
	Y	0.22	0.25
	Z	0.13	0.05

Table 2.1: *RMSE of the 2D-3D registration algorithm for the two prothesis components. For the reconstruction, the exact volumetric data of the implant was hereby used.*

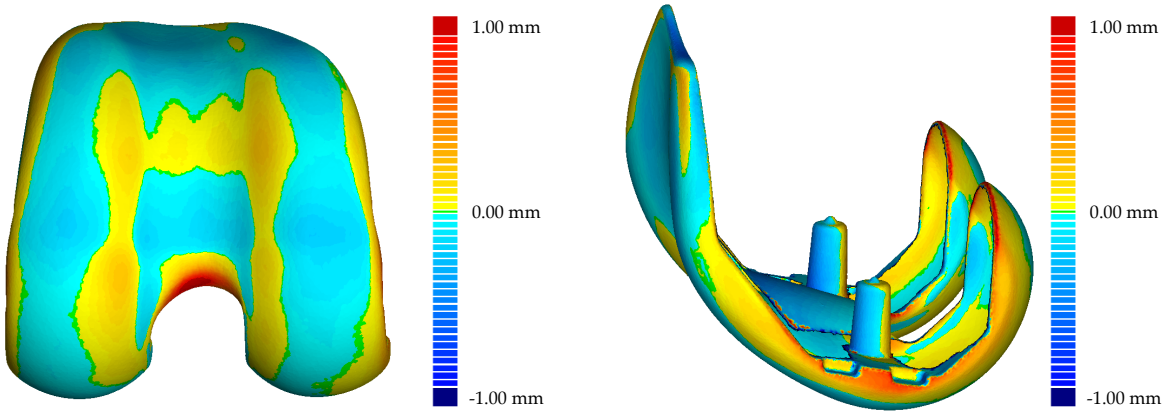

(a) Bottom view (b) Side view

Figure 2.11: *The above pictures depict the surface discrepancy of the manufactured prothesis component with respect to the CAD construction data.*

plant was first placed at the aforementioned distance and then shortened by 0.1 mm, the corresponding image size would then shrink. In order to keep the same image, the object would have to be moved at a focus distance of 897.0 mm. Therefore, if the change of the original size was not known a priori, an error of 3.0 mm would arise in the estimation procedure of the out-of-plane position (figure 2.12).

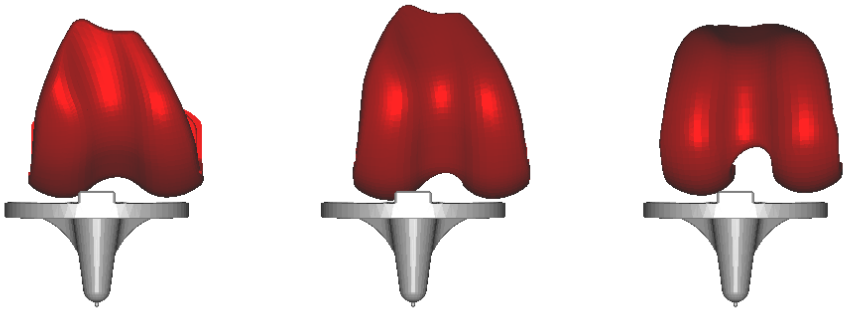

Figure 2.12: *In the above images, the erroneous shift of the femur component with respect to the tibia in out of plane direction is caused by inaccurate volumetric data.*

2.2.5 Mobile Fluoroscopy

In section 1.3, it is rationalized that in order to acquire the kinematics of the knee joint during daily activities by means of video fluoroscopy, the imaging system has to be displaced by an automated moving device.

Horizontal motion

The mobile system developed at the Institute for Biomechanics of the ETH Zurich was first conceived to track subjects during level walking. The approach was to construct an automated cart to which the video fluoroscope can be attached. The developed cart is able to measure the distance of the knee relative to the line of sight of the fluoroscope and to minimize it. Therefore, the knee joint is constantly kept in the field of view of the image intensifier.
The first prototype that was used for the study conducted by Zihlmann et al. [123] was able to track the knee joint merely during the stance phase of level walking. The traction was transferred by a single motor, that drove an axle connecting two of the four wheels by means of a transmission chain. The maximal velocity and acceleration that could be achieved was $2.5\,\mathrm{m/s}$ and $4\,\mathrm{m/s^2}$ respectively, which is clearly not enough for tracking the knee during a complete stride. Therefore, the design had to be improved. For the new prototype, four electrical motors were installed. Each motor drives exactly one wheel through an epicyclic gear with a gear ratio of 1:20. In order to guarantee a straight motion, the motors were electronically configured to act as unit, thus creating two electric live axles connected to each other. Precisely, one motor is defined as a master, while the other ones, configured as slaves, adjust their position according to the motion of the former.
The four wheels are arranged in such a way, that the cart is optimally stabilized at all times. Due to the high accelerations during measurements, the weight of the cart is not completely homogeneously distributed over the wheels. Therefore, the motor that is mainly subject to the greatest load was chosen as the master drive. Furthermore, in order to maximize the traction, the wheels were specially fabricated and hooped with a high friction polymer.
The relative position of the knee joint to the center of the imaging unit is tracked by means of a draw wire sensor, which is screwed onto the automated cart right underneath the C-arm. The end of the wire is attached to a strap around the knee (figure 2.13). The output signal is extended to an external computer, which instantly

records the excursion of the wire. The computer exploits this knowledge to drive the motors according to a feedback controller to keep the knee joint in the field of view of the video fluoroscope.
The automated fluoroscope has now a maximal horizontal velocity and acceleration of 3.5 $^{m}/_{s}$ and 8 $^{m}/_{s^2}$ respectively [39, 36].

Vertical motion

The wire sensor was modified to measure the orientation of the wire in relation to the imaging plane. At the wire exit a bar was constructed as guidance. Moreover, the bar joint was equipped with a potentiometer to instantly measure the direction of the wire (figure 2.14). This information is then exploited to calculate the position of the knee relative to the principal axis of the fluoroscopic projection. The automated unit was equipped with a ball bearing linear guide on each side of the fluoroscope (figure 2.15). The vertical progression accounts to 2 mm per revolution. The controlled vertical motion was achieved by two electrical motors and is analogously designed as the horizontal drive, i.e. the two slides are synchronized at all time to move as unit. The master drive was virtually designed in the controlling software and directly operates according to the controlling algorithm. This adds a new degree of freedom to the movement of the fluoroscopic equipment and makes it possible to track the knee joint during combined horizontal and vertical displacement, such as during stair descent (figure 2.16)[37].
The C-arm of the fluoroscope was equipped with reflective markers, five on the X-ray source and seven on the image intensifier. As described in section 2.2.3, the X-ray

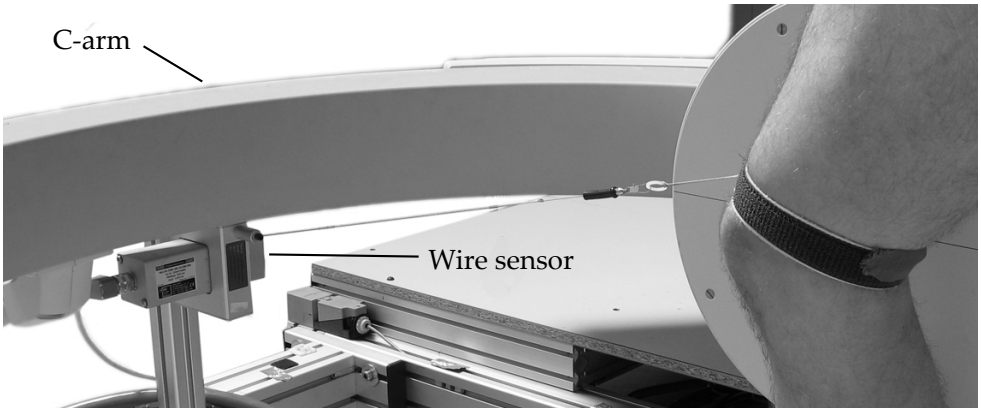

Figure 2.13: *The wire sensor measures the position of the knee relative to line of sight of fluoroscope by means of a strap.*

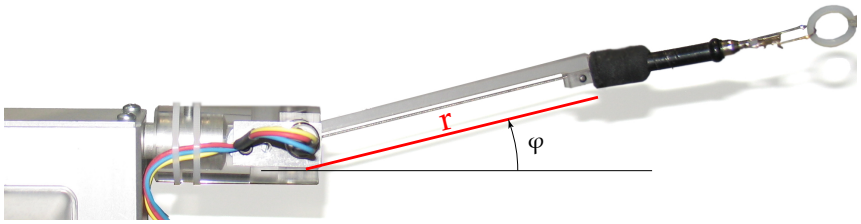

Figure 2.14: *The potentiometer at the base of the bar measures the orientation of the wire.*

imaging system is calibrated with respect to the video-photogrammetric equipment. Therefore, by tracking the markers fastened to the C-arm, the relative orientation and location of the reference frame of the fluoroscope are also known during any displacement inferred by the automated system.

Security concept

Since the measurements involve human beings, the robot unit has been built with a high level of safety.
As in many industry applications that involve human interactions, the automated fluoroscopic equipment was conceived to come to an immediate stop if the emergency circuit is cut. During the whole measurement, two operators are exclusively responsible for the safety of the subject. They are equipped with an emergency button which works according to the *dead man* principle. Therefore, the robot unit operates only when the button is being pressed.

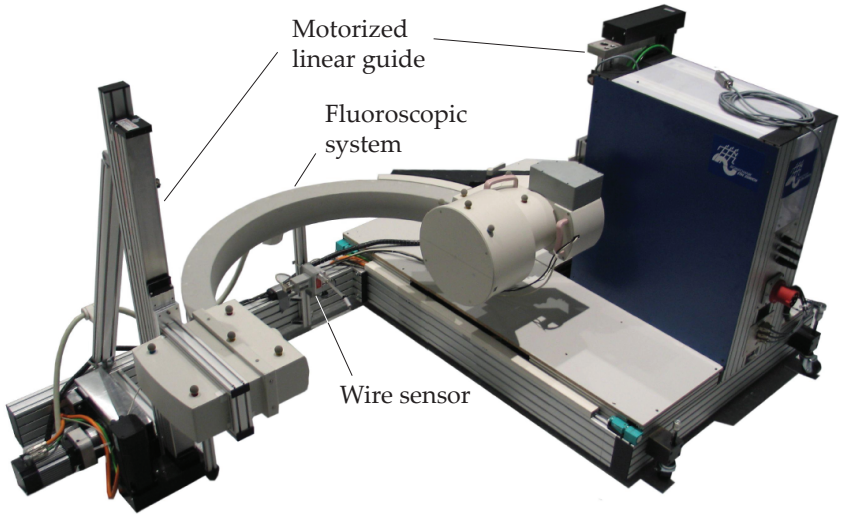

Figure 2.15: *The automated moving fluoroscope developed and used during this project.*

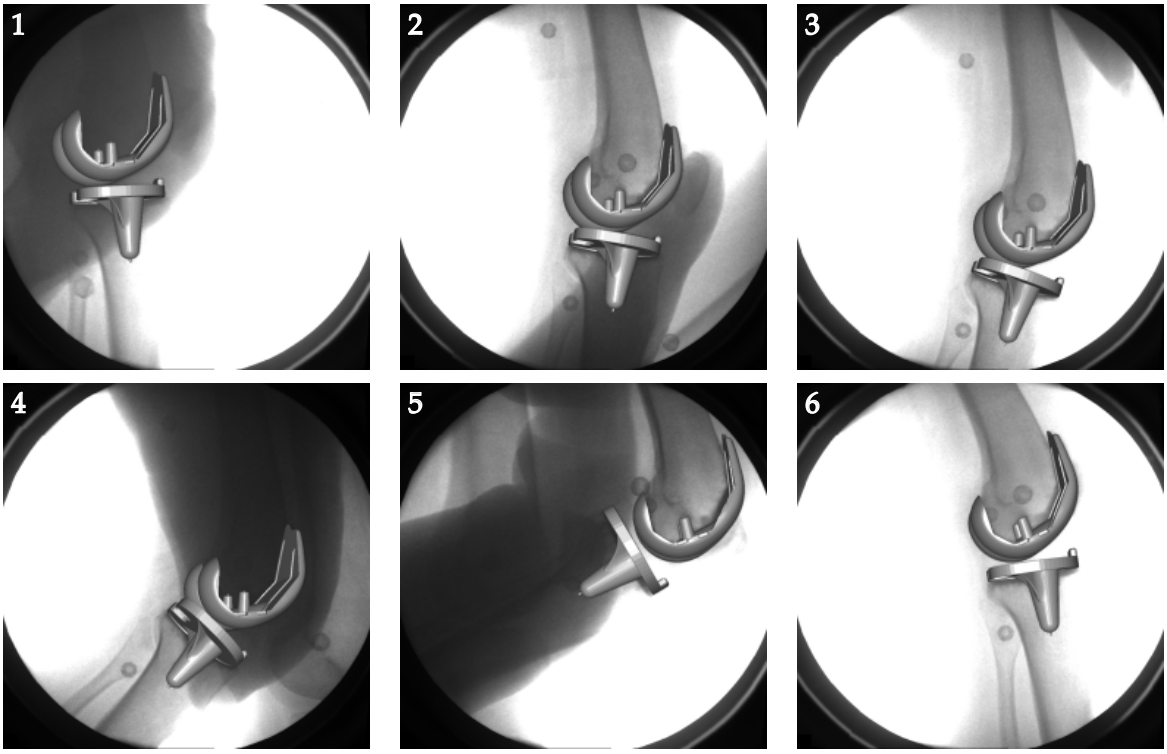

Figure 2.16: *Full stride of stair gait. The images are the result after 2D to 3D registration. The series corresponds to selected radiographs from a full trial acquisition at 25 frame/s. Every 7^{th} frame was chosen for the above sequence.*

Furthermore, the whole system is designed to be double-fail safe. In other words, in case of an emergency, the automated fluoroscopic equipment can be efficiently brought to a quick stop even if two individual components are malfunctioning. In addition, the displacement of the two vertical slides is not only supervised by the controlling PC, but also by a microcontroller installed in the robot unit. Hereby, the two vertical axes are constantly synchronized, even in case of a breakdown.
During measurement, the robot unit is electronically restricted to keep a unique course. This exploits the fact that the knee joint primarily moves in direction of locomotion; thus there is no need for the mobile equipment to invert its movement. By this means, an erroneous controlling output cannot result in a condition during which the automated fluoroscopic equipment actively runs into the subject walking in the middle of the C-arm.
As with all the X-ray equipments, special attention needs to be addressed to the radiation exposure of the subject involved in a fluoroscopy based biomedical study. Accordingly to the manufacturer, 60 seconds of pulsed fluoroscopy corresponds to approximately 0.12 mSv. The Swiss Federal Office of Public Health sets the limit for

the yearly accepted dose at 5 mSv. A measurement trail relates to approximately 3 seconds of pulsed fluoroscopy. Therefore, a study consisting of 10 trails per subject corresponds to 30 seconds of radiation, thus 1.2% of the yearly accepted dose.
The measurements carried out in this project are been approved by ethic committee of the ETH Zurich.

2.3 Instrumented Stairs

In the field of biomechanics, it is common practice to combine video photogrammetry and force plates in order to gather useful mechanical data for a complete human movement analysis.
During gait, irregularity of the walking ground causes the subject to adapt to the surface; therefore deviation of level gait can be observed. In order to minimize this kind of bias and to avoid any accident because of tripping and falling over, force plates are usually installed either in the ground or a in the middle of particularly designed walkway.
The gait analysis lab of the Institute for Biomechanics is equipped with six force plates installed in the ground and two mobile ones, thus providing an overall smooth and even surface to walk on. The particularity of this gait lab is, that the force measurement was conceived to minimize the mechanical sources of disturbances. The idea behind this concept was to decouple the six fixed force plates from the surrounding floor by installing them on a concrete pillar, which was previously constructed on top of the building basement. Moreover, a damping material was interposed at the very bottom of the pillar to reduce incoming vibrations (figure 2.17). Such a complex provides the prerequisites for an accurate retrieval of ground reaction forces.
The mobile force plates are employed for stair activities measurements. They are inserted in two steps of a particularly designed staircase which is placed in the middle of the lab during data retrieval. In contrast to the 6 fix in place force plates, the staircase bears directly on the floor. Therefore, a kinetic data acquisition combined with moving fluoroscopy imaging would be irreparably compromised because of the secondary vibrations induced by the moving fluoroscope assembly. This matter of concern was settled by developing a new staircase that can be fastened alongside the other force plates, thus preventing any crosstalk coming from the surrounding floor. Each step of the stairway measures 280mm, 180mm and 800mm in depth, height and width respectively. Because of the restriction to 3 steps, no stair rails were mounted (figure 2.18). Thereby, the stairs are liable to the regulation of the Swiss Office for

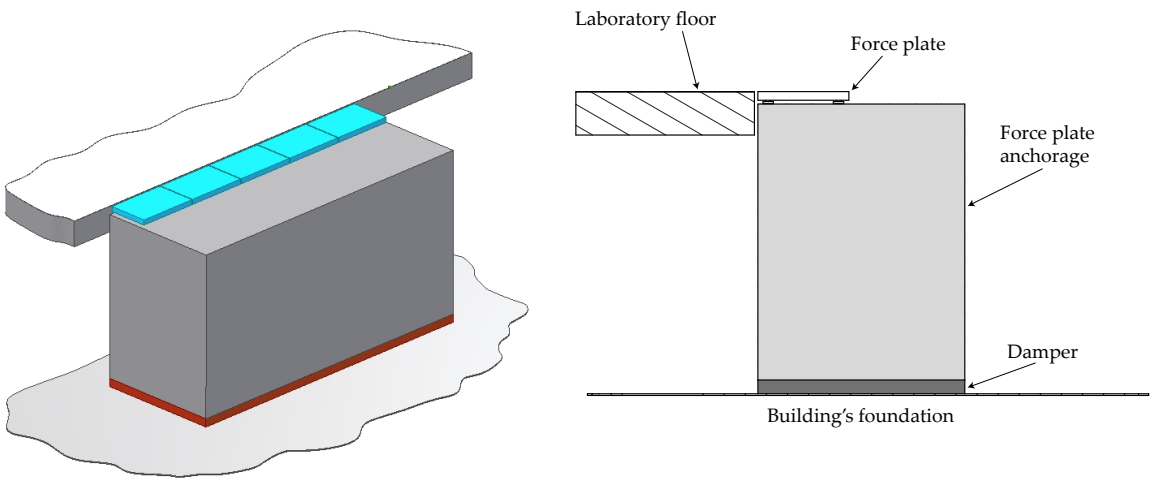

Figure 2.17: *Force plate assembly at the IfB gait analysis lab*

Accident Prevention[3].

2.3.1 Errors of Force Plate Data

The force plates used in this project are portable multi-component force plates Type 9286AA manufactured by Kistler Instruments Corporation[4]. The top surface is where

[3]For more informations see `www.upi.ch/PDFLib/725_43.pdf`
[4]For more informations please see `www.kistler.com`

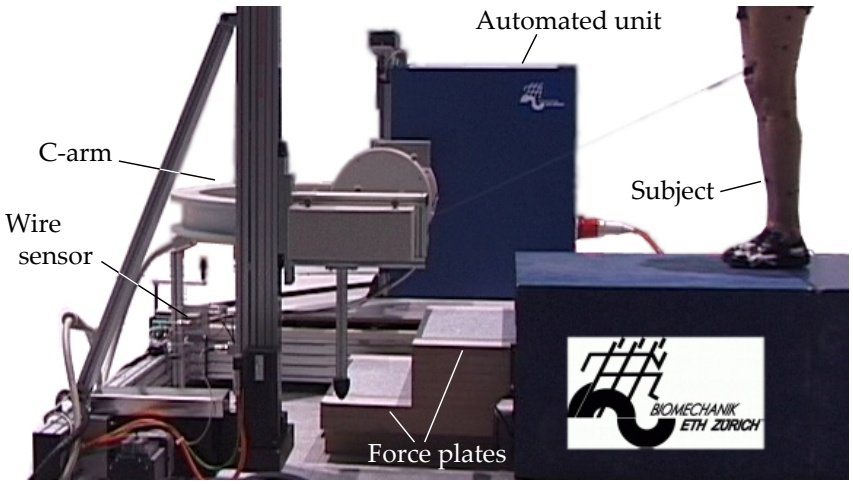

Figure 2.18: *The set up for stair measurements with moving video fluoroscopy. As shown in the above image, the staircase is placed in the middle of the walkway.*

the subject applies the pressure during gait and has a dimension of 600x400 mm. The force measurements is carried out by four piezoelectric sensor blocks arranged at the corners of the plate. Each sensor embodies three quartz crystal plates that are respectively sensitive to thrusts in the three orthogonal directions. The signals coming from the sensors are gathered and conducted to an internal charge amplifier. The signals generated by horizontal shears are arranged in pairs, thus after defining the coordinate system as in figure 2.19, the outputs carried to the data acquisition computer are equivalent to eight force components F_{z1}, F_{z2}, F_{z3}, F_{z4}, F_{x1+x2}, F_{x3+x4}, F_{y1+y4}, F_{y2+y3}. According to the manufacturer, with the know distances a and b of the sensor center relative to the midpoint of the plate, the resultant moments are calculated as

$$M_x = b \cdot (F_{z1} + F_{z2} - F_{z3} - F_{z3}) \tag{2.7}$$

$$M_y = a \cdot (-F_{z1} + F_{z2} + F_{z3} - F_{z4}) \tag{2.8}$$

$$M_z = b \cdot (-F_{x1+x2} + F_{x1+x2}) + a \cdot (F_{y1+y4} - F_{y2+y3}) \tag{2.9}$$

The system of forces can be statically reduced to a resultant force $F = (F_x, F_y, F_z)^t$ applying at the center of pressure[5] (COP) and a couple T_z perpendicular to the plate. The COP can be calculated as follows:

$$a_x = \frac{F_x \cdot a_z - M_y}{F_z} \tag{2.10}$$

$$a_y = \frac{F_y \cdot a_z + M_x}{F_z} \tag{2.11}$$

where a_z is given by the manufacturer and represents the depth of the sensor measurement relative to the force plate surface.

[5]The center of pressure corresponds to the intersection point of the force F with the surface of the force plate.

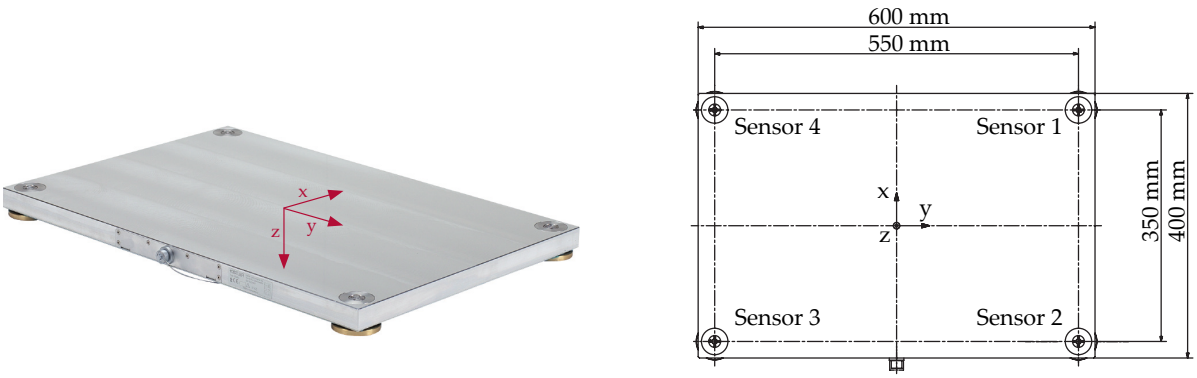

Figure 2.19: *Definition of the dimensions and parameters of the Kistler force plate 9286AA*

According to Dettwyler [30], the signals of the force plates exhibit a significant crosstalk between each other and hence are prone to a systematic error. He showed that through appropriate calibration, the error for the evaluation of the COP can be considerably reduced ($|\Delta a| \leq 1\,\text{mm}$). For the couple T_z resulting from the force F_M induced by a subject M, the error amounts to $|\Delta T_z| \leq 0.3\,\text{mm} \cdot F_M$.
The calibration procedure consisted in applying a force changing over time at 66 predefined points on the surface of the force plate. In order to prevent conveying any torque and hence to introduce sources of error, the tool for force application consisted of a pointed bar on the user side and a notched plated on the force plate side (figure 2.20). Since the exact location of the several centers of pressure were known a priori, the correction coefficients could be assessed over the entire surface of the force plate by means of a least-squares optimization [30].
Although the center of pressure for the conveyed force can be corrected, the direction of the force vector still shows a substantial error. Previous investigations [122] report mean errors of up to 2 degrees. For a knee joint at a distance of 500 mm from the ground, such a deviation induces a miscalculation of the lever arm for knee joint moment analysis of up to 17 mm. Considering that the position of the knee implant components can be determined with a deviation less than 2 mm (section 2.2.4), it can clearly be noted that, for an accurate computation of knee mechanics, it is imperative to reduce the error of the measured kinetics. Therefore, the force plate calibration procedure had to be refined in order to ameliorate the calculation of the force orientation. The calibration bar was optimized by adding a rotational joint at its upper end, where the user applies a random force in direction of the force plate. This guarantees that only forces along the center line of the bar are conveyed to the calibration point. In order to track the direction of the bar and thus of the applied force at all time, eight reflective markers were screwed at well defined positions along the bar[6] (figure 2.21).
The original applied force $\mathbf{F}$ can be calculated out of the measured force $\widehat{\mathbf{F}}$ and an unknown term that reflects the crosstalk of the sensor signals and is dependent on the surface location of the center of pressure on the force plate. This can be mathematically described with the following equation:

$$\mathbf{F} = \widehat{\mathbf{F}} + \Delta\mathbf{F}(x, y) \tag{2.12}$$

[6]Hereby, it is important to note that the calibration bar was constructed with a precision of 0.1mm.

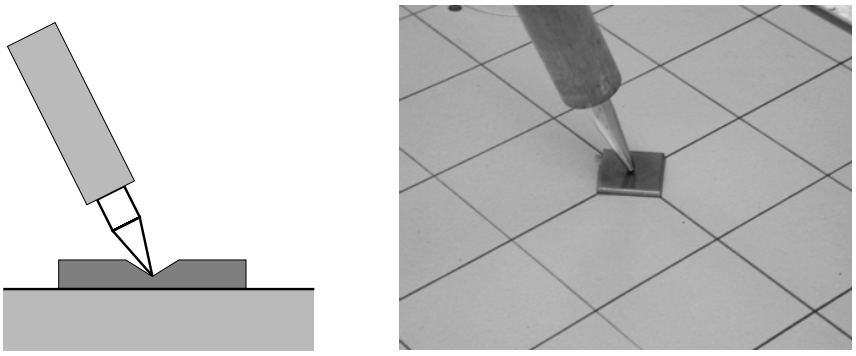

Figure 2.20: *In order to convey exclusively a punctual force, the calibration rod ends with a pointed tip. Furthermore, a notched plate is placed between the tip of the rod and the force plate to prevent any damage to the surface of the plate.*

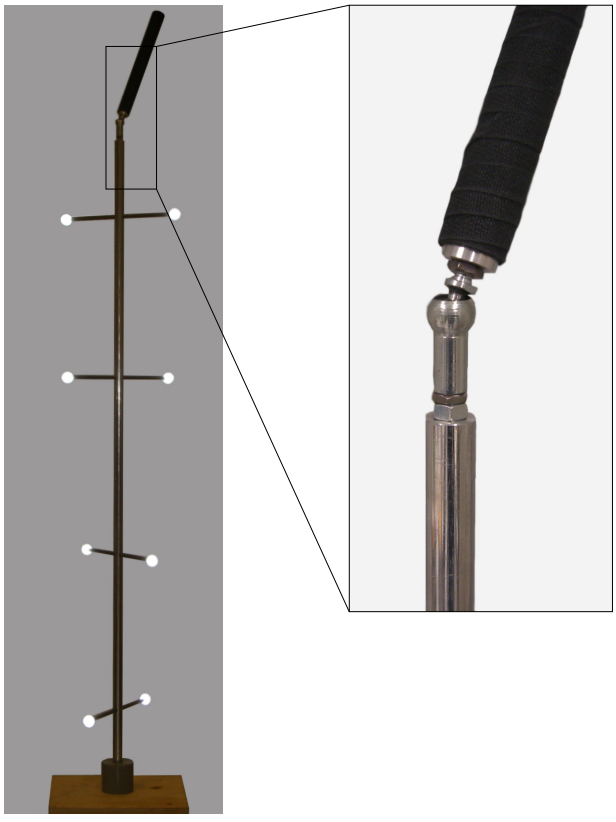

Figure 2.21: *The above rod was specifically constructed for the calibration of the force plates. On the left, it can be noted how the markers are distributed along the bar. The right pictures emphasizes the rotation joint added to ensure that forces are exclusively conveyed along the bar.*

$\Delta\mathbf{F}(x, y)$ can be derived out of the measured force $\widehat{\mathbf{F}}$ multiplied with some unknown correction coefficients. Thus, it follows:

$$\mathbf{F} = \widehat{\mathbf{F}} + \begin{pmatrix} c_{x\to x} & c_{y\to x} & c_{z\to x} \\ c_{x\to y} & c_{y\to y} & c_{z\to y} \\ c_{x\to z} & c_{y\to z} & c_{z\to z} \end{pmatrix}_{(x,y)} \widehat{\mathbf{F}} \tag{2.13}$$
$$\mathbf{F} = \widetilde{\mathsf{C}}_{(x,y)}\widehat{\mathbf{F}}$$

where $\mathbf{F}$ denotes the true force and $\widehat{\mathbf{F}}$ the measured force.
During calibration, the user constantly changed the direction of the bar and thus the force application in order to collect as many information as possible about the behavior of the signal crosstalk[7]. Therefore, by rewriting equation 2.14, the correction coefficient matrix $\widetilde{\mathsf{C}}_{(x,y)}$ can be computed for the acquired N samples in the following way:

$$\mathbf{F} = \begin{pmatrix} \widehat{\mathbf{F}}_1 & 0 & 0 \\ 0 & \widehat{\mathbf{F}}_1 & 0 \\ 0 & 0 & \widehat{\mathbf{F}}_1 \\ \widehat{\mathbf{F}}_2 & 0 & 0 \\ 0 & \widehat{\mathbf{F}}_2 & 0 \\ 0 & 0 & \widehat{\mathbf{F}}_2 \\ \vdots & \vdots & \vdots \\ \widehat{\mathbf{F}}_N & 0 & 0 \\ 0 & \widehat{\mathbf{F}}_N & 0 \\ 0 & 0 & \widehat{\mathbf{F}}_N \end{pmatrix} \begin{pmatrix} \tilde{c}_{x\to x} \\ \tilde{c}_{y\to x} \\ \tilde{c}_{z\to x} \\ \tilde{c}_{x\to y} \\ \tilde{c}_{y\to y} \\ \tilde{c}_{z\to y} \\ \tilde{c}_{x\to z} \\ \tilde{c}_{y\to z} \\ \tilde{c}_{z\to z} \end{pmatrix} \tag{2.14}$$

$$\mathbf{F} = \widehat{\mathsf{F}}\,\tilde{\mathbf{c}} \tag{2.15}$$

where $\mathbf{F}$ is given by the magnitude of the measured force and the direction of the calibration pole, $\widehat{\mathbf{F}}_k = (f_{kx}, f_{ky}, f_{kz})$ defines the measured force at k-th frame and $\tilde{c}_{x,y,z\to x,y,z}$ are the correction coefficients for the given center of pressure.
The above system of equations consists of 9 independent variables and N linear equations, with $N \gg 9$. Since the system is overdetermined, $\tilde{\mathbf{c}}$ is calculated out of the pseudo inverse of $\widehat{\mathsf{F}}$, thus resulting in the least square solution for the problem.
For each of the 66 predefined points of pressure, the correction matrix $\widetilde{\mathsf{C}}_{(x,y)}$ was computed. In order to be able to correct the forces over the entire force plate, the correction coefficients were parameterized with a four degree polynomial.

[7]The sampling rate for the analog signals coming from the force plate sensors amounted to 2000 Hz, while the position of the reflective markers was sampled at a frequency of 200 Hz.

In figure 2.22, the angle difference between the calculated direction of the force application by means of the force plate signals and the direction of the calibrating bar is shown for the whole plate surface before and after calibration.
This correction algorithm considerably diminishes the systematic error that arises during the force measurements, as shown in figure 2.23.

2.4 Experimental Protocol

Two subjects, a 78 year old female and a 72 year old male[8], who underwent a total knee arthroplasty during the past 6 years, were recruited to participate in this study. The former did not show any impairment or any pain related to the joint implant. The latter complained over not localized discomfort and difficulties with deep flexion. However, both of the subjects were able to freely perform daily activities without the need of any sort of external assistance. Before the experiment, each subject gave his written informed consent.

[8]For the sake of simplicity, in chapter 3, the subjects, who took part in the study, are referred to as *FELE30* and *BAPI36*.

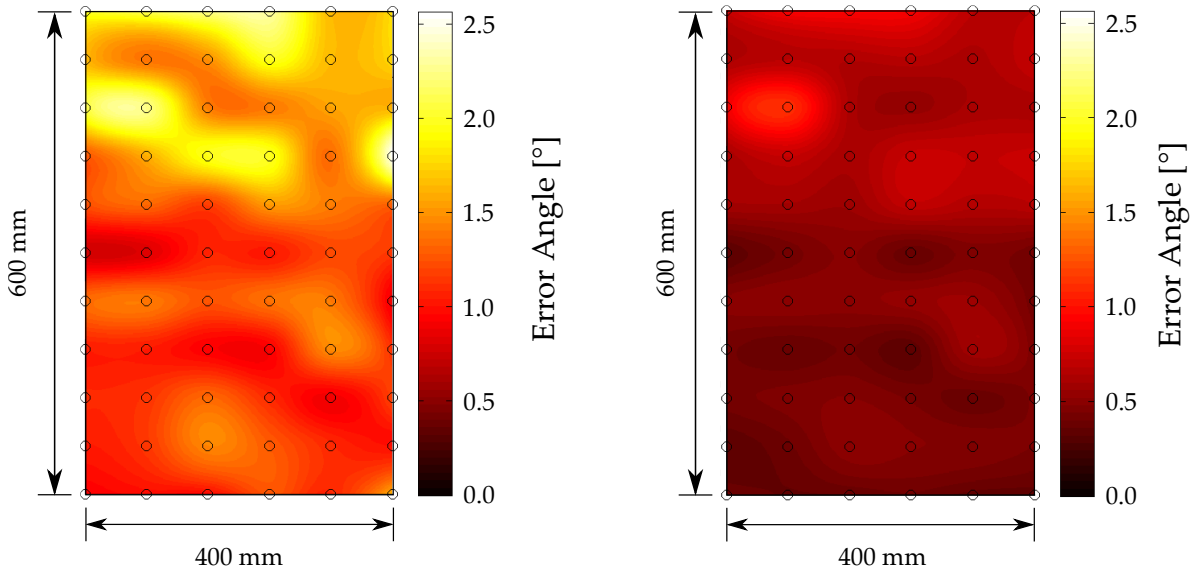

Figure 2.22: *The above temperature graphs report the angle between the force vector measured by the force plate and the direction of the calibration rod before (left) and after (right) calibration.*

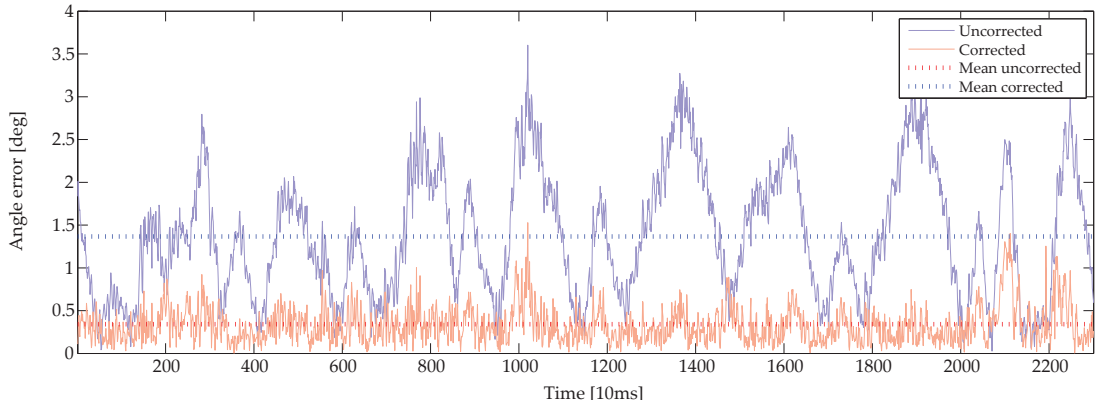

Figure 2.23: *Angle between the force vector and the direction of the calibration rod at a predefined location on the force plate before and after correction.*

2.4.1 Outline

Almost every biomechanical laboratory independently develops its own marker set for human motion analysis based on video photogrammetry [2, 17, 75]. The choice of such a set is dependent on a variety of factors, which all have an impact on how well the movement of the underlying structure, i.e. the position and orientation of the bones, are determined.
The marker set used for this study was assessed by Institute of Biomechanics of the ETH Zurich (figures 2.24 and 2.25)[69]. The main developing criteria were the following: 1. marker number per segment, 2. marker positioning relative to each other and to the segment areas most affected by soft tissue artifacts and 3. marker visibility with respect to the motion capture cameras. Each marker is attached directly onto the skin, therefore no external fixations are needed. Each segment is provided with a minimum of 6 markers, i.e. 7 for the pelvis, 6 for the thigh, 6 for the shank, 9 for the foot.

2.4.2 Coordinate Systems Definitions

The measured quantities during a mechanical assessment are expressed in the specific reference frame of the measuring equipment. In this study, since different types of

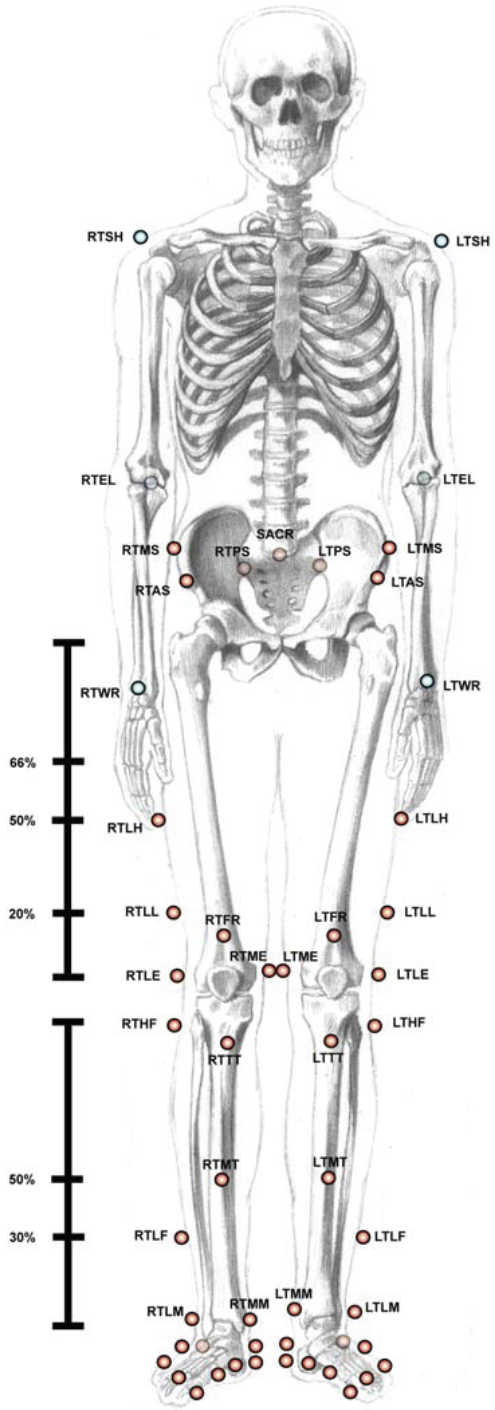

Code	Description
RTSH	Right shoulder
LTSH	Left shoulder
RTEL	Right elbow
LTEL	Left elbow
RTWR	Right wrist
LTWR	Left wrist
SACR	Sacrum
RTPS	Right posterior iliac spine
LTPS	Left posterior iliac spine
RTMS	Right middle iliac spine
LTMS	Left middle iliac spine
RTAS	Right anterior iliac spine
LTAS	Left anterior iliac spine
RTLH	Right lateral thigh high
LTLH	Left lateral thigh high
RTLL	Right lateral thigh low
LTLL	Left lateral thigh low
RTFR	Right frontal thigh
LTFR	Left frontal thigh
RTLE	Right lateral epicondyle
LTLE	Left lateral epicondyle
RTME	Right medial epicondyle
LTME	Left medial epicondyle
RTHF	Right high fibular head
LTHF	Left high fibular head
RTTT	Right tuberositas tibiae
LTTT	Left tuberositas tibiae
RTMT	Right mid tibia
LTMT	Left mid tibia
RTLF	Right lateral fibula
LTLF	Left lateral fibula
RTLM	Right lateral malleolus
LTLM	Left lateral malleolus
RTMM	Right medial malleolus
LTMM	Left medial malleolus

Figure 2.24: *Full marker set*

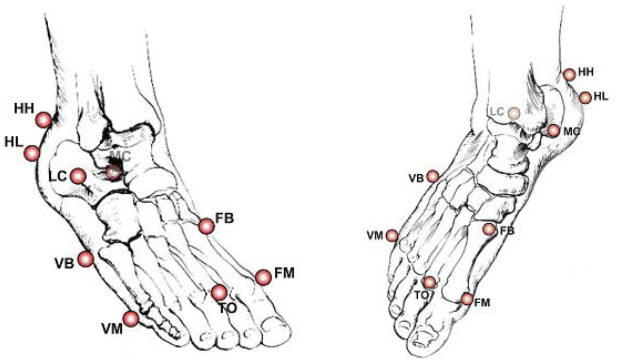

Code	Description
HH	High heel
HL	Low heel
MC	Medial calcaneus
LC	Lateral calcaneus
VB	Proximal head of fifth metatarsal
VM	Distal head of the fifth metatarsal
TO	Distal head of the second metatarsal
FB	Proximal head of the first metatarsal
FM	Distal head of the first metatarsal

Figure 2.25: *Foot marker set*

instrumentations are combined and synchronized to each other, it is imperative that each coordinate system is precisely defined and that the corresponding spatial transformation is known at all time with respect to the global reference frame.

Global reference frame

The world coordinate system of the Vicon measuring equipment is defined as the global reference frame. The direction of walking is mapped onto the y-axis, the vertical displacement is described by the z-axis and movements towards the side of locomotion by the x-axis.
The orientation of the ground reaction forces measured by the force plates is expressed in terms of the global reference frame. The corresponding alignment is computed during initialization and calibration of the photogrammetric equipment.

X-ray imaging reference frame

The X-ray imaging system is separated in two reference frames. The first one describes the image coordinates in pixels, while the other defines the actual orientation and location of the imaging equipment. For simplicity, the image plane is spanned by the x and y-axis and the z is thus collinear with the principal axis of the cone beam (figure 2.26).

TKA reference frame

Each component of the knee implant has its own coordinate system definition.
The z-axis was chosen such that a sagittal projection of the components would form if

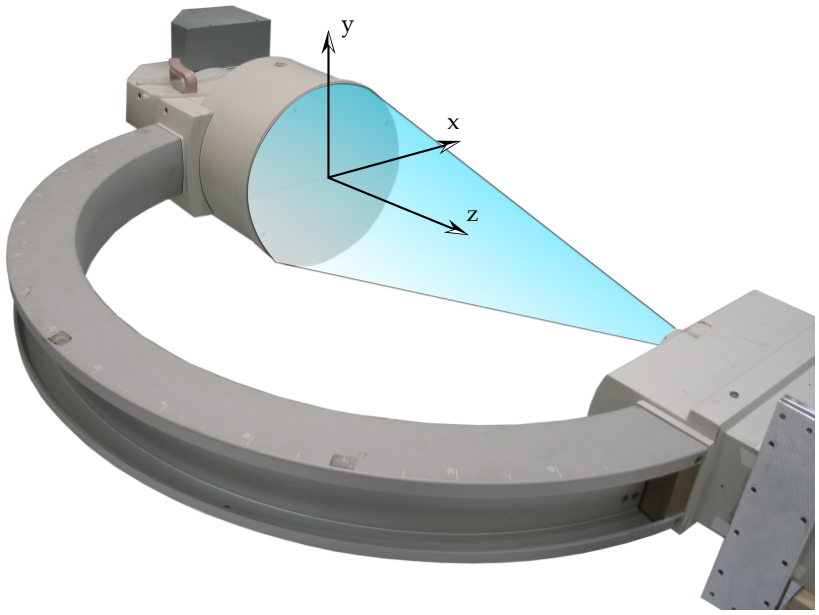

Figure 2.26: *Coordinate system of the X-ray imaging system*

the axis was aligned with the principal axis of the fluoroscopic imaging.
The origin of the reference frame of the femoral component was chosen to lie in the middle of the two condyles and on the construction axis of the curvature of the running surface (figure 2.27). For the tibial component, the most distal point on the surface of the implant was defined as the origin.

2.4.3 Data Acquisition

At the beginning of each experiment, the subjects were given time to get accustomed to the automated fluoroscopic system, i.e. during this time the X-ray equipment was turned off and the subject performed the requested activity without being exposed to radiation. According to the feedback received by the subjects participating in this and previous studies [123], they report feeling completely comfortable with the moving equipment after approximately 2 to 4 trials. However, no detailed biomechanical investigation was done to assess whether the gait is significantly altered or affected by the automated fluoroscopic system.
For every experimental trial, each subject was asked to perform a minimum of 5 strides starting from the top of the staircase descending down and continuing along the walkway. This way, stair stepping, transition from stair to ground floor and level walking were all combined in the same measurement trail (figure 2.28). Ground reac-

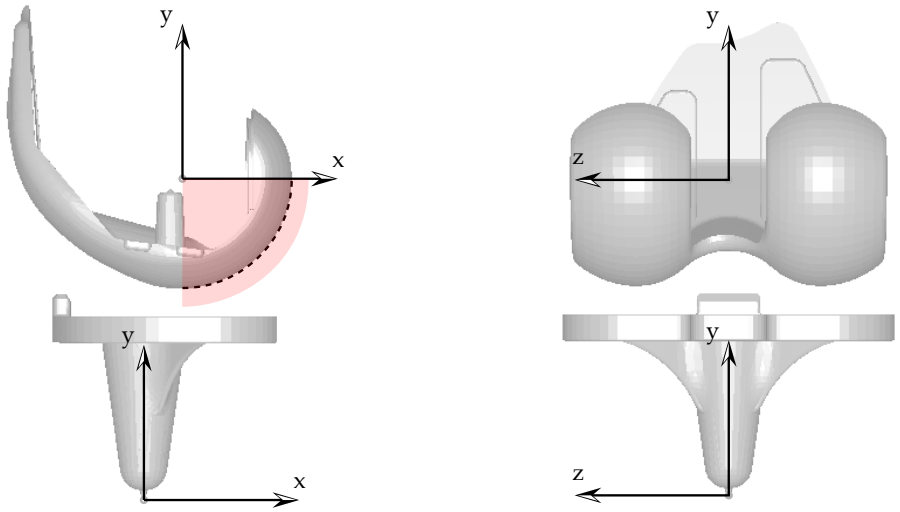

(a) Antero-posterior (b) Medio-lateral

Figure 2.27: *Coordinate systems of the total knee replacement for 2D to 3D reconstruction. The red arc represents the curvature of the running surface of the femoral component for a flexion angle of* 0° *to* 90°.

tion force measurements, motion capture and fluoroscopic imaging were performed synchronously.

2.4.4 Data Processing

Ground reaction force

In order to compare the measurements carried out in this study with previous reports, several parameters were defined in order to characterize the trajectory of the ground reaction force (figure 2.29). The determination of the parameters was based on the routine after Stüssi et al. [104, 111].
F_{z1} which defines the impact peek at touch down was not relevant for this study. Therefore, F_{z2} represented the first peak during weight acceptance. F_{z4} referred to the second maximum during the final phase of stance, i.e. during push-off. F_{z3} was defined at the local minimum between F_{z2} and F_{z4}, thus describing unloading at mid-

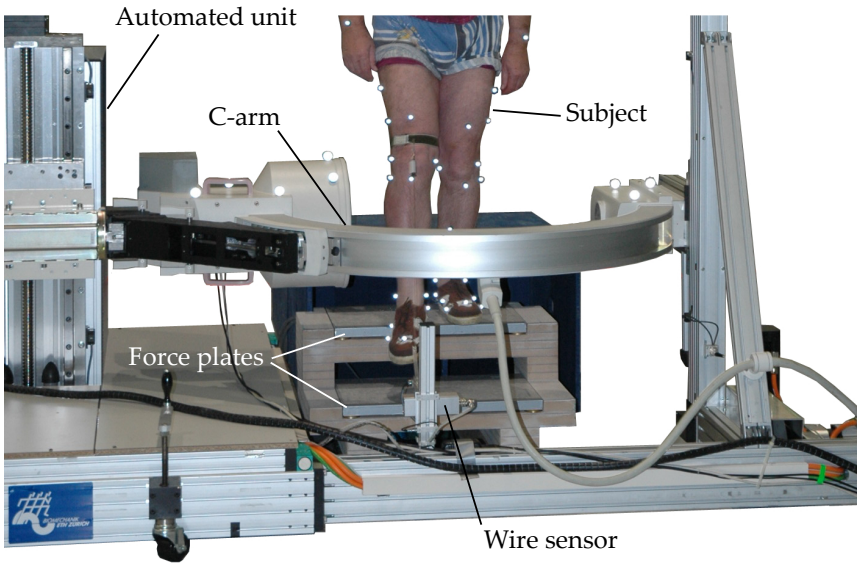

Figure 2.28: *Frontal view of a measurement trail*

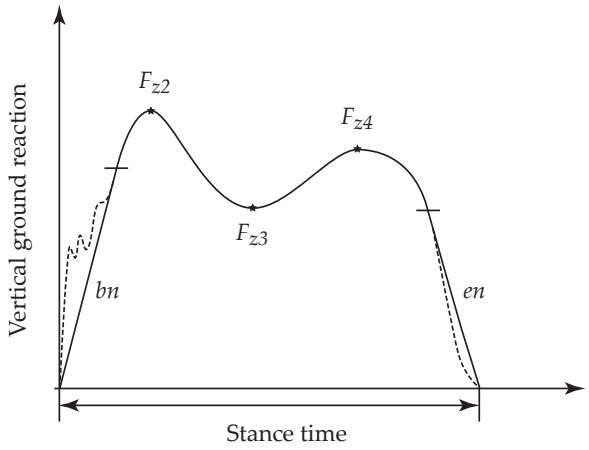

Figure 2.29: *Vertical ground reaction force parameters. F_{z2} and F_{z4} stand for the two local maxima, and F_{z3} for the local minimum at midstance. The loading and unloading rates are defined by the parameters bn and en, respectively.*

stance.

Knee joint rotations

The rotations assessed by means of video photogrammetry were described by the motion of the thigh with respect to the shank. Each segments was identified by the

corresponding marker cluster. In order to determine, the flexion axis of the knee relative to the segment clusters, the subject performed fifteen isolated weight bearing knee bends. The recorded movements were analyzed by a computer optimization, and the axis of rotation that best reproduced the knee flexion was defined as the knee joint axis. The adduction-abduction axis was described by the vector perpendicular to the knee joint axis and the line connecting the knee joint center and the ankle joint center. The internal-external axis of rotation was determined by the vector that formed an orthonormal basis with the flexion-extension and adduction-abduction axes [69].
The axis that described the flexion-extension of the knee implant by means of fluoroscopic data was chosen to lie on the z-axis of the femoral component, i.e. the the line passing through the lateral and medial centers of curvature of the femoral condyles. This definition reflects the geometrical axis that describes the motion of the normal tibio-femoral joint [40]. The femoral internal-external rotation was described by the rotation about the longitudinal axis of the tibia, while the varus-valgus rotation corresponded to the rotation in the frontal plane of the tibial component.

Knee joint moment calculation

In gait analysis, it is common practise to estimate the net joint forces and moments by means of inverse dynamics. Thereby, each segment i is modeled as a rigid body with mass m_i and is mutually connected with another segment k with mass m_k.
By defining the examination coordinate system as stationary, the equations of motion for the segment i are given as follows [52],
for the change of linear momentum

$$\sum_k \mathbf{F}_{ki} + \mathbf{F}_{ei} + m_i\mathbf{g} = \frac{d}{dt}(m_i\mathbf{v}_i) = m_i\mathbf{a}_i \tag{2.16}$$

and for the change of angular momentum

$$\sum_k (\mathbf{r}_{ki} \times \mathbf{F}_{ki}) + (\mathbf{r}_{ei} \times \mathbf{F}_{ei}) + (\mathbf{r}_i \times m_i\mathbf{g}) + \sum_k \mathbf{M}_{ki} + \mathbf{M}_{ei} = \frac{d}{dt}[(\mathbf{r}_i \times m_i\mathbf{v}_i) + \mathsf{I}_i\boldsymbol{\omega}_i], \tag{2.17}$$

where $\mathbf{F}_{ki}$ and $\mathbf{M}_{ki}$ denotes the reaction force and moment of segment k on i, $\mathbf{F}_{ei}$ and $\mathbf{M}_{ei}$ the net external force and moment acting on segment i, while $\mathbf{r}_{i,ei,ki}$ describes the respective positions relative to origin of the reference frame. $\mathbf{M}_{ei}$ account also for the mechanical influence of the passive structures of the joint (e.g. ligaments and joint capsule) and the muscles.
The principle of inverse dynamics is to start distally from the measured ground reaction forces and moments and proceeding proximally by analyzing segment after

segment [46]. Therefore, the equations of motion for N segments are given by

$$\begin{aligned}\sum_i \mathbf{F}_{ei} + \sum_i m_i \mathbf{g} &= \frac{d}{dt}\sum_i (m_i \mathbf{v}_i) \\ \sum_i \mathbf{F}_{ei} &= \sum_i m_i \mathbf{a}_i - m_{\text{tot}}\mathbf{g}\end{aligned} \tag{2.18}$$

and

$$\sum_i (\mathbf{r}_{ei} \times \mathbf{F}_{ei}) + \sum_i \mathbf{M}_{ei} = -\sum_i (\mathbf{r}_i \times m_i \mathbf{g}) + \sum_i (\mathbf{r}_i \times m_i \mathbf{a}_i) + \sum_i \frac{d}{dt}(\mathrm{I}_i \boldsymbol{\omega}_i). \tag{2.19}$$

Moving the reference observation point from the origin to $\mathbf{r}_{kl}$, the location of the joint between segment k and l, the net joint moment is defined as

$$\begin{aligned}\mathbf{M}_{lk} = &\underbrace{-(\mathbf{r}_r - \mathbf{r}_{lk}) \times \mathbf{F}_r}_{1} + \underbrace{\sum_{i=1}^{k}[(\mathbf{r}_i - \mathbf{r}_{lk}) \times m_i \mathbf{g}]}_{2} \\ &+ \underbrace{\sum_{i=1}^{k}[(\mathbf{r}_i - \mathbf{r}_{lk}) \times m_i \mathbf{a}_i]}_{3} + \underbrace{\sum_{i=1}^{k} \frac{d}{dt}(\mathrm{I}_i \boldsymbol{\omega}_i)}_{4}\end{aligned} \tag{2.20}$$

In many clinical investigations, where slow walking speed are requested, the first term of equation 2.20 may contains sufficient information [52].
Neglecting term 3 and 4 gives a quasistatic approximation of the model. This gives sensible results without undue error for gait speeds up to $5\,\mathrm{m/s}$ [62, 119]. Therefore, in this study, the net knee joint moment calculation is reduced to the first two terms of equation 2.20.

Error analysis

For a given function $f(x_1, x_2, \ldots, x_n)$ the corresponding variance σ_f^2 is derived as follows,

$$\sigma_f^2 = \sigma_{x_1}^2 \frac{\partial f}{\partial x_1} + \sigma_{x_2}^2 \frac{\partial f}{\partial x_2} + \cdots + \sigma_{x_n}^2 \frac{\partial f}{\partial x_n} \tag{2.21}$$

Therefore, the variance σ_M^2 for the for the first term of the net joint moment calculation in equation 2.20 can be calculated. Defining $\mathbf{r} = \mathbf{r}_r - \mathbf{r}_{kl}$, it follows that

$$\mathbf{M} = \mathbf{r} \times \mathbf{F} = \begin{pmatrix} r_y F_z - r_z F_y \\ r_z F_x - r_x F_z \\ r_x F_y - r_y F_x \end{pmatrix} \tag{2.22}$$

Therefore, the corresponding variance is given by

$$\sigma_M^2 = \begin{pmatrix} \sigma_{r_y}^2 F_z^2 + \sigma_{F_z}^2 r_y^2 + \sigma_{r_z}^2 F_y^2 + \sigma_{F_y}^2 r_z^2 \\ \sigma_{r_z}^2 F_x^2 + \sigma_{F_x}^2 r_z^2 + \sigma_{r_x}^2 F_z^2 + \sigma_{F_z}^2 r_x^2 \\ \sigma_{r_x}^2 F_y^2 + \sigma_{F_y}^2 r_x^2 + \sigma_{r_y}^2 F_x^2 + \sigma_{F_x}^2 r_y^2 \end{pmatrix} \tag{2.23}$$

with the respective variances

$$\sigma_{r_x}^2 = \sigma_{\mathrm{CoP}_x}^2 + \sigma_{\mathrm{CoR}_x}^2 + \sigma_{\mathrm{Vicon}}^2 \tag{2.24}$$

$$\sigma_{r_y}^2 = \sigma_{\mathrm{CoP}_y}^2 + \sigma_{\mathrm{CoR}_y}^2 + \sigma_{\mathrm{Vicon}}^2 \tag{2.25}$$

$$\sigma_{r_z}^2 = \sigma_{\mathrm{CoP}_z}^2 + \sigma_{\mathrm{CoR}_z}^2 + \sigma_{\mathrm{Vicon}}^2 \tag{2.26}$$

where σ_{CoP}^2 is the variance of the center of pressure on the force plate, σ_{CoR}^2 defines the variance of the position of the center of rotation of the knee joint, which is computed by the registration algorithm, and $\sigma_{\mathrm{Vicon}}^2$ the variance for the coordinates of the marker locations determined by means of motion capture. Hereby, it is to note that the above sources of error are independent to each other and can be added together without further due.
The standard deviations for the above measurement parameters are indicated in table 2.2.
In order to illustrate the order of magnitude of the root mean squared error propagation of the measuring system, σ_M^2 has been calculated for the flexion moment exhibited by the subjects involved in the study and plotted against the mean of the moment and the corresponding standard deviation (figure 2.30). It is visible that σ_M^2 is significantly smaller that the variability of the flexion moment of both subjects.

Statistical analysis

For the study, two independent subjects were recruited. Since for both subject no assumption was made about the distributions of the moments and rotations at the

Measured variable	RMSE
Center of pressure (x, y)	1 mm
Center of rotation (y, z)	0.28 mm
Center of rotation (x)	1.02 mm
Marker location (Vicon)	1 mm
Ground reaction force	$1\% \cdot mg$

Table 2.2: *Standard deviation of the error sources in the measuring equipment*

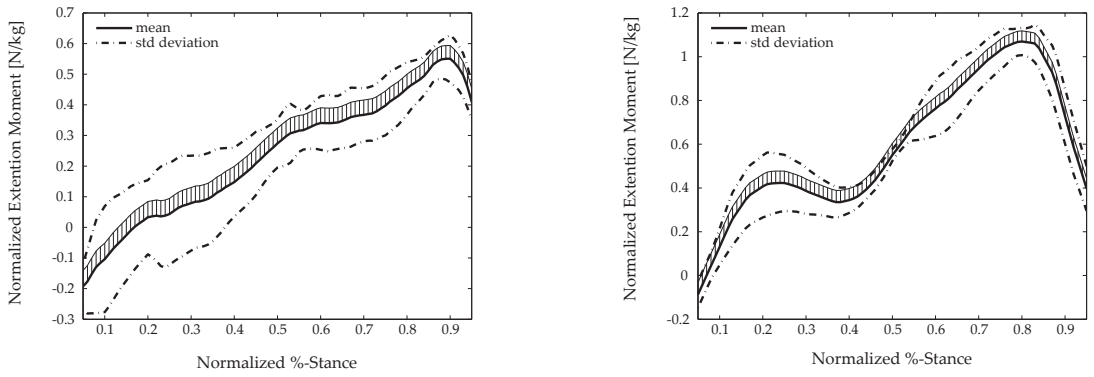

(a) BAPI36 (b) FELE30

Figure 2.30: *Extension knee joint moment plotted for the subject* BAPI36 *and* FELE30*. The thick line defines the mean of the trails, while the intermittent one represents the corresponding standard deviation. The root mean squared error of the measured data is emphasized by the vertical lines.*

knee joint, the non-parametric Mann-Whitney U-test was used to evaluate the several observations. Significant difference was set at a conservative $p < 0.05$.

However beautiful the strategy,
you should occasionally look at the results.

Winston Churchill (1874 - 1965)

3 Experimental Results

In this chapter, the results of the measurements of stair descent are presented. After the description of the computed findings, a respective discussion will follow. The data was acquired and processed according to the procedure described in section 2.4.
Unless otherwise stated, values are expressed by their mean with the corresponding standard deviation enclosed in parenthesis.

3.1 Knee Joint Kinematics

This section presents the rotations registered at the knee joint during the measurement trials. Shown are flexion, adduction and internal rotation of the femur relative to the tibia.

3.1.1 Video Fluoroscopy

The flexion angle of the knee for *BAPI36* started off at -10° during touch down and was constant for the first 20% of the stair cycle and it slowly increased to approximately 20° for the next 40%. Then, it quickly rose to a maximum of about 60° between 60-75% of the stair cyle. During this time, the knee transitioned from stance to swing phase. It then fully extended for the remaining of the stride (figure 3.1).
At heel strike, *FELE30* flexed the knee from 0° to 5-10° during the first 10% of stride

and kept the same angle for the next 20% of cycle time. Then, the flexion gradually increased and reached a maximum of approx. 70° little after toe off, which occurred at about 70% of stride. During the remaining time, the knee returned to full extension (figure 3.2).
BAPI36 showed a slight adduction with a maximum of 1° during stance. During swing phase, the variation of the varus-valgus rotation over all the trials showed an evident increase compared to stance.
FELE30 exhibited a quite stable and neutral adduction pattern during stance. The swing phase brought a valgus displacement in the knee with a maximum of about 2° at mid swing.
The internal rotation of *BAPI36* had its maximum at full flexion. A tendency to rise with flexion could be identified. However, a remarkable increase in variability could be noted during the swing phase.
The femoral component in *FELE30* did not show any evident change in internal rotation during stance. Nonetheless, a constant external rotation of about 2° was observed. At toe off the femur rotated 7° externally up to 50% of the swing phase. In the second half, it returned to its initial position.
The total range of motion of flexion, varus and internal rotation performed by *BAPI36* amounted to $83.2°(3.5)$, $2.8°(0.4)$ and $6.0°(1.7)$, respectively. *FELE30* showed ranges of motion in the order of $84.6°(1.9)$, $3.1°(0.7)$ and $6.8°(0.8)$ (figure 3.3).

3.1.2 Video Photogrammetry

The trajectory of the flexion for both subjects was very similar to the one evaluated by means of fluoroscopic data. In *BAPI36*, an evident shift was present. The range of motion shown here were $73.9°(3.2)$ and $77.1°(1.3)$ for *BAPI36* and *FELE30*, respectively.
During stance, *BAPI36* did not exhibit a large movement about the varus-valgus rotation axis. A tendency of an opposite motion with respect to the data determined by means of fluoroscopy was noted. During swing, the knee rotated in valgus direction for about 2°. In this interval, the trajectory presented two local maxima. *FELE30* also showed little varus-valgus rotation during stance. After toe off, the knee adducted for approximately 3°. Two local maxima were visible even in this case.
For the subject *BAPI36*, the internal-external rotation at stance demonstrated an opposite trajectory compared to fluoroscopic data. The knee rotated internally. At 60% of the stair cycle, an internal rotation was initiated and reached a maximum at about 75%.
For the complete stance phase of the subject *FELE30*, the femur component constantly rotated internally. At toe off, a maximal external rotation of about 5° was observed.

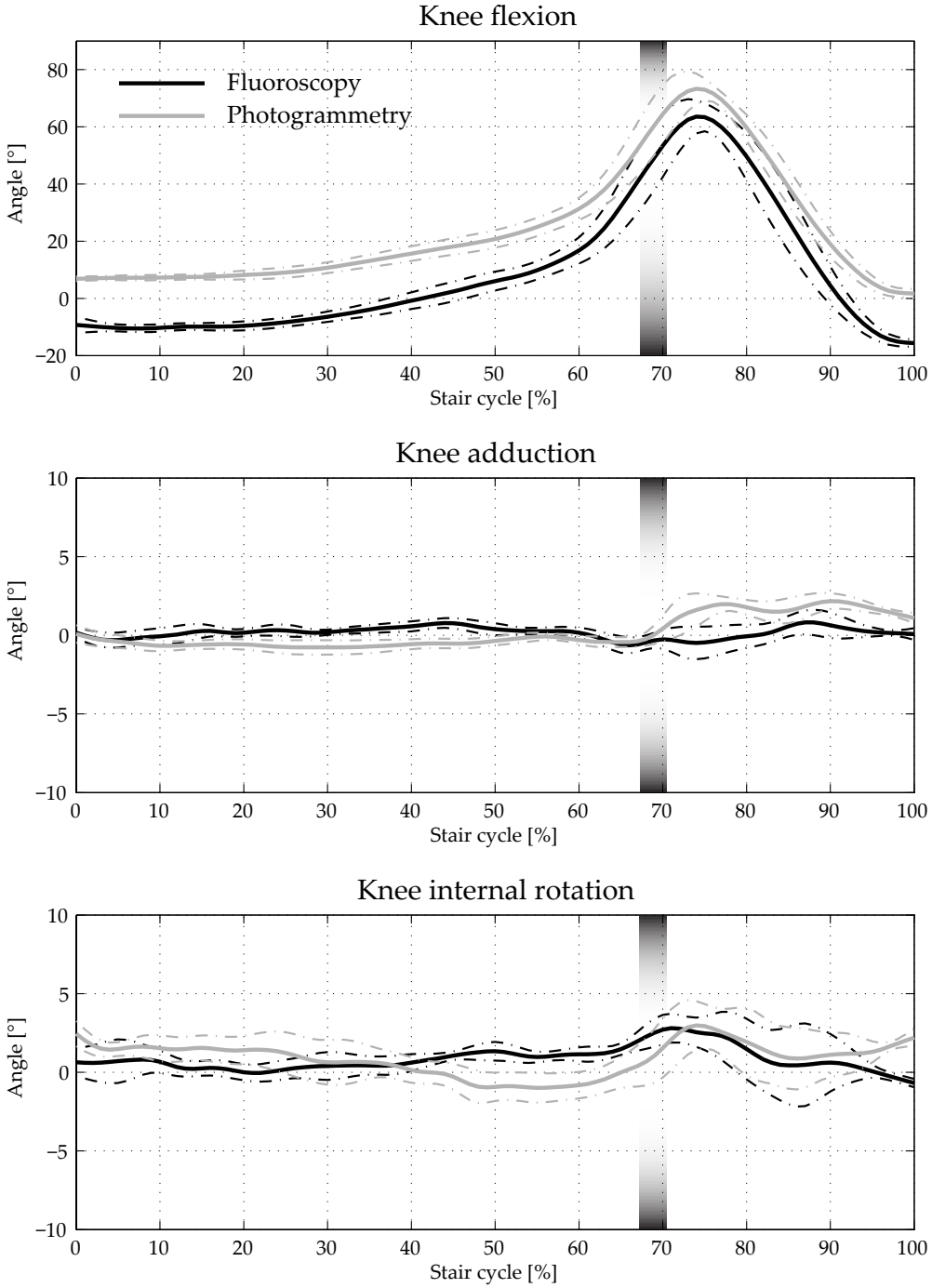

Figure 3.1: *(BAPI36) Rotation angles at the knee joint determined by means of fluoroscopic (black) and photogrammetric (gray) measurements. The solid and the dotted line represent the mean and the corresponding standard deviation over five trials. The vertical grey bar indicates the variation of the toe off event.*

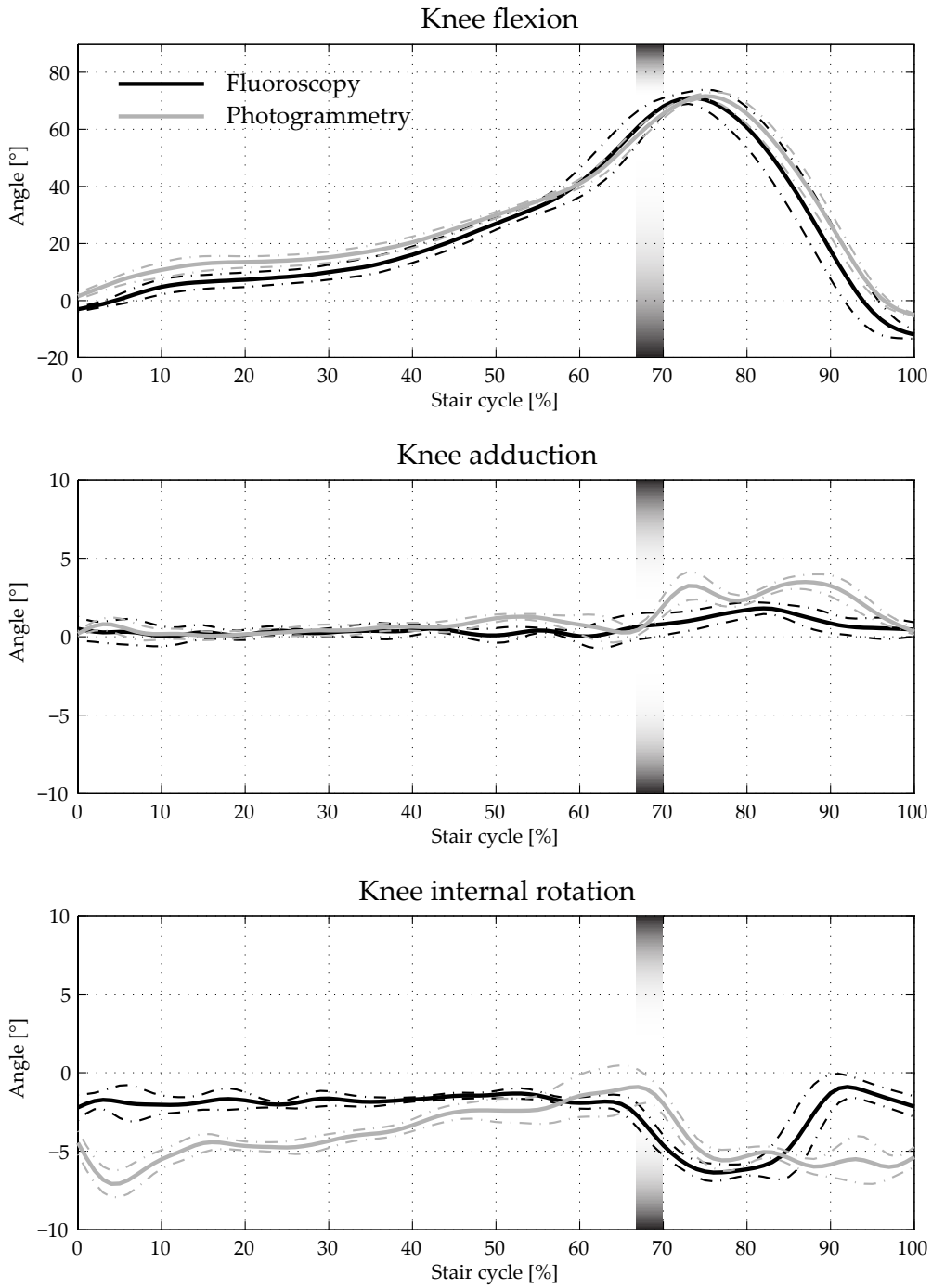

Figure 3.2: *(FELE30) Rotation angles at the knee joint determined by means of fluoroscopic (black) and photogrammetric (gray) measurements. The solid and the dotted line represent the mean and the corresponding standard deviation over five trials. The vertical grey bar indicates the variation of the toe off event.*

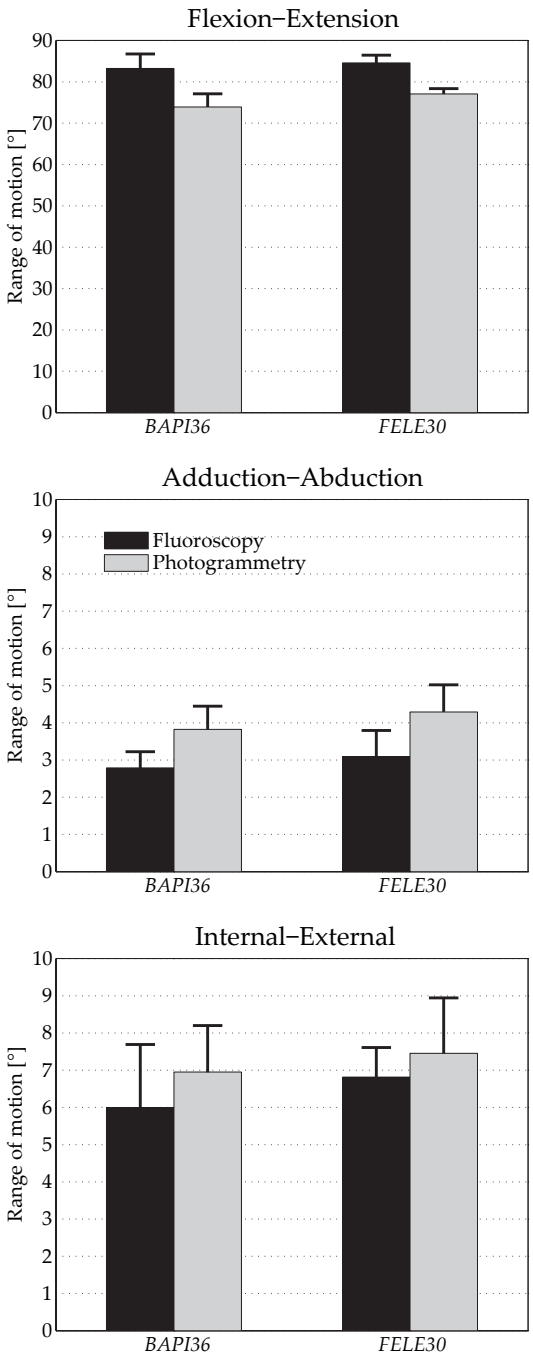

Figure 3.3: *Ranges of motion for flexion-extension, adduction-abduction and internal-external rotation registered at both subjects. The black and gray bars indicate the mean values with the corresponding standard deviation observed with video fluoroscopic and video photogrammetric data, respectively.*

3.2 Knee Joint Kinetics

The net moment acting on the knee joint was calculated according to the first two terms of equation 2.20 described in section 2.4.4. For a better understanding, the moment was then split in three components, i.e. extension, adduction and axial moment.
As in the previous section, the results computed by means of video fluoroscopic data are first presented and then compared with video photogrammetry based calculations.

3.2.1 Video Fluoroscopy

In the first 10% of the stance phase, *BAPI36* exerted a flexion moment. For the rest of the stance, the subject increasingly applied an extension moment at the knee joint to reach a maximum at about 90% of stance. A rather extended variability was observed over the trials (figure 3.4). Registered was a mean maximal extension moment of $0.59(0.05)\,\mathrm{Nm/kg}$ (table 3.1).
The subject *FELE30*, in contrast to *BAPI36*, exhibited two local maxima in the trajectory of the extension moment, one at 25% and the other at 85% of stance (figure 3.5). The moment variability was less pronounced than in *BAPI36*. The mean maximal value was determined at $1.13(0.03)\,\mathrm{Nm/kg}$.
In the first 15% of stance, a steady increase of the adduction moment was denoted in *BAPI36*. A slight double waveform could be observed in the trajectory. During the last 40% of stance, the adduction moment constantly decreased.
FELE30 showed a local minimum at adduction moment in the first 10% of stance. The trajectory then quickly rose to its maximal mean value of $0.34(0.06)\,\mathrm{Nm/kg}$ within 5%. In contrast to the subject *BAPI36*, a triple waveform was present in the pattern of the adduction moment.
Compared to the intensity of the other net moment components, the mean axial moment registered for *BAPI36* reached far lower values (table 3.1). The highest amplitudes were registered between 10% and 50% of the stance period. On the contrary, the subject *FELE30* exhibited a more extended axial moment. A clear and prolonged maximum was registered at about 85% of stance.

3.2.2 Video Photogrammetry

The pattern of net knee joint moments calculated by means of video photogrammetric data were very similar to the trajectories displayed by the results of the video fluoro-

Moment [Nm/kg]		*BAPI36* Max value	*BAPI36* Min value	*FELE30* Max value	*FELE30* Min value
Extension	*Photo*	0.61(0.06)	−0.02(0.06)	1.09(0.01)	−0.67(0.02)
	Fluoro	0.59(0.05)	−0.11(0.07)	1.13(0.03)	−0.11(0.03)
Adduction	*Photo*	0.33(0.02)	0.03(0.05)	0.40(0.07)	−0.06(0.06)
	Fluoro	0.37(0.04)	0.04(0.05)	0.34(0.06)	−0.08(0.06)
Axial	*Photo*	−0.01(0.01)	−0.08(0.01)	0.14(0.02)	−0.03(0.01)
	Fluoro	0.04(0.01)	−0.01(0.01)	0.14(0.03)	−0.02(0.01)

Table 3.1: *Maximal and minimal values of the extension, adduction and axial net joint moments registered over the measurement trials for the two subjects. The results were calculated with video photogrammetric (Photo) and video fluoroscopic (Fluoro) data.*

scopic measurements evaluations. This is also confirmed by the mean maximal and minimal values registered for all moment components, as summarized in table 3.1. The difference in mean moment magnitude resulted to lie primarily between one standard deviation for the flexion and adduction moment of both subject and for the axial moment of *FELE30*. Considerably well reproduced by the video photogrammetric data were also the different moment variabilities of the trials. However, a discernible discrepancy in trajectory could be observed at the axial moment calculated for the subject *BAPI36*. During the whole stance period, the moment showed an opposite pattern than the one calculated by means of video fluoroscopic data.

3.2.3 Ground Reaction Forces

The pattern of the ground reaction force in anterior-posterior direction was similar for both subjects and showed the same characteristics as in the case of level walking (figure 3.6)[111].
The force decreased at touch down to a minimum of about 10% the bodyweight in the direction of travel, thus absorbing the forward acceleration of the body. During most of the stance phase, the force steadily increased and reached his maximum of 15% bodyweight in the opposite direction of travel at toe off. For both subjects, the transfer from a negative to positive force occurred approximately at mid stance and characterizes the forward propulsion of the body.
The vertical force exhibited a different progression between the two subjects (figure 3.7). For *BAPI36*, the force reached its first maximum, defined as Fz_2 (section 2.4.4), relative quickly and then immediately dropped to about one bodyweight. For most

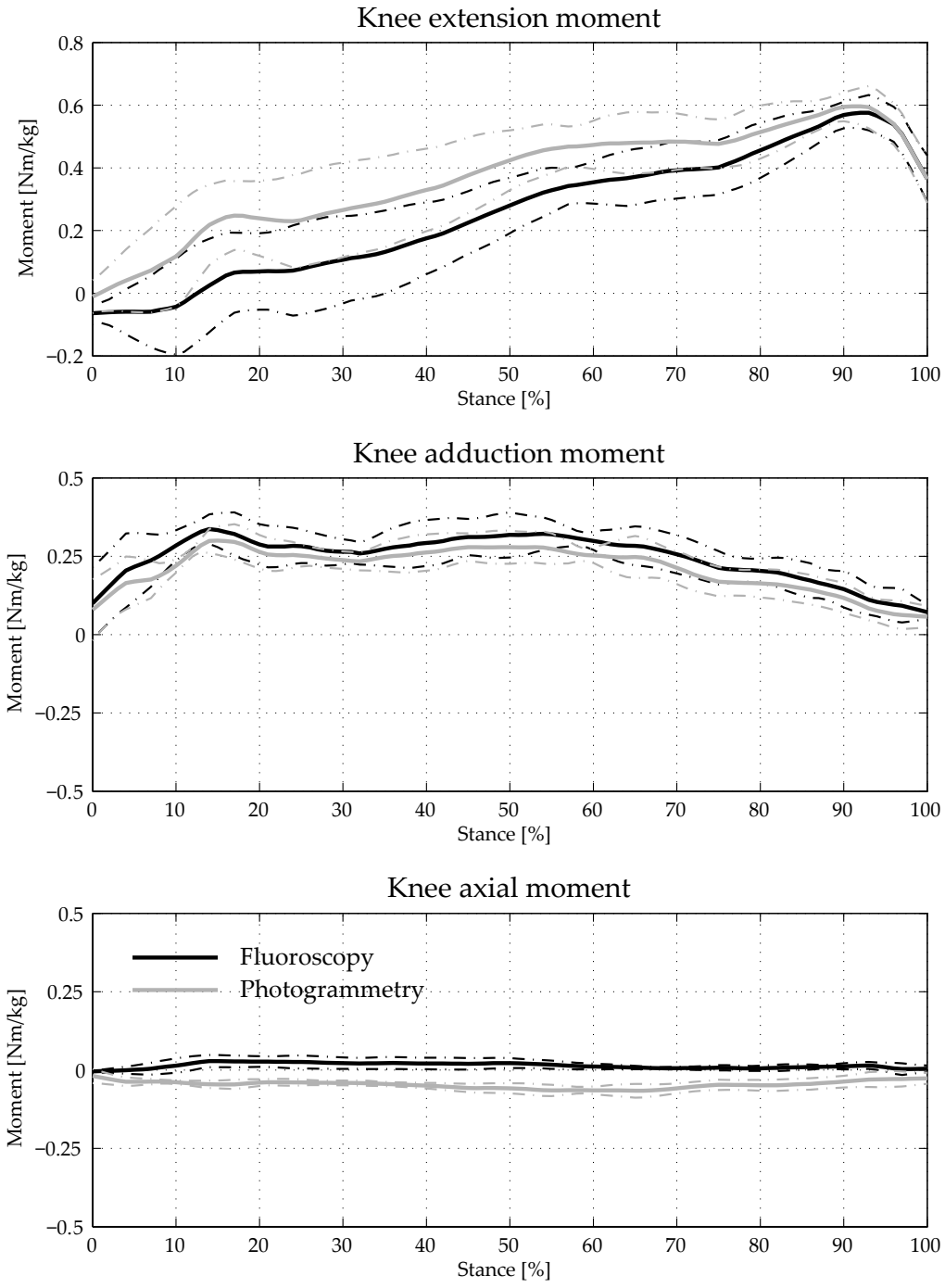

Figure 3.4: *(BAPI36) Net moments at the knee joint determined by means of fluoroscopic (black) and photogrammetric (red) measurements. The solid and the dotted line represent the mean and the corresponding standard deviation over five trials. The stance phase is defined for the interval during stance when the vertical ground reaction is greater than a threshold of 100 N.*

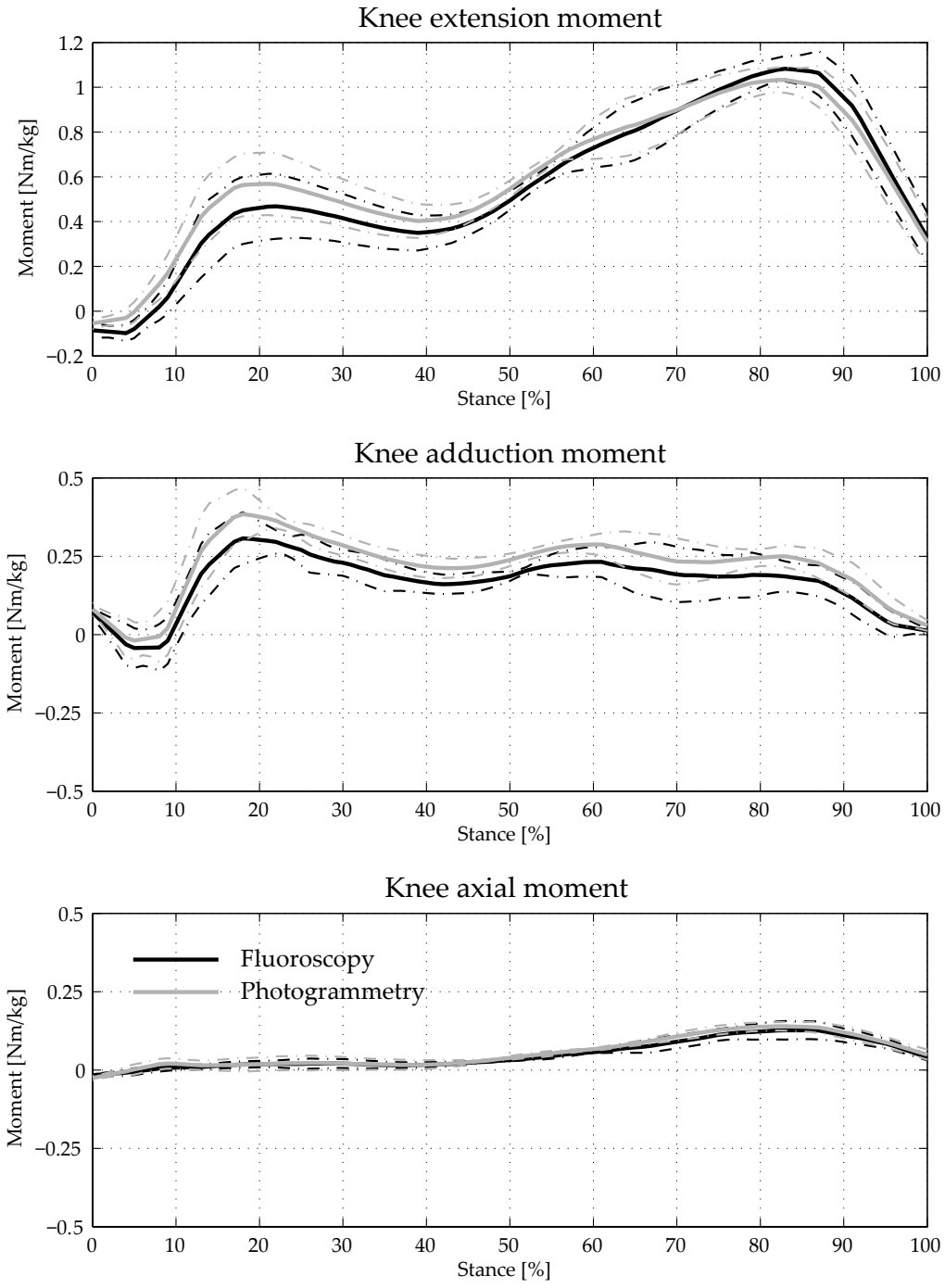

Figure 3.5: *(FELE30) Net moments at the knee joint determined by means of fluoroscopic (black) and photogrammetric (red) measurements. The solid and the dotted line represent the mean and the corresponding standard deviation over five trials. The stance phase is defined for the interval during stance when the vertical ground reaction is greater than a threshold of 100 N.*

part of the stance phase, the vertical load at the force plate barely changed and smoothly transitioned to the final unloading interval. Qualitatively, the minimum Fz_3 was situated early on during stance as opposed to level walking, during which Fz_3 approximately occurs at mid stance. Furthermore, the second peak Fz_4 was not detectable.

The vertical force exerted at *FELE30* rose to Fz_2 at a comparable rate and to an analogous bodyweight magnitude as *BAPI36*. However, a fast decrease to a local minimum was not visible in this case. Instead, the force slowly declined to a plateau of one bodyweight, thus making Fz_3 and Fz_4 undetectable. Moreover, the unloading phase prior toe-off started later on as opposed to the slow transition in *BAPI36*.

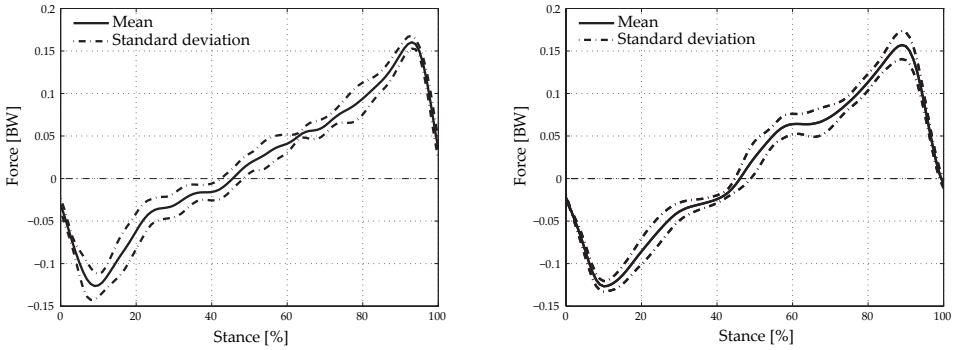

(a) BAPI36 (b) FELE30

Figure 3.6: *Anterior-posterior ground reaction force registered for the both subjects. Displayed are the mean (continuous line) and the standard deviation (intermittent line) over all the trials.*

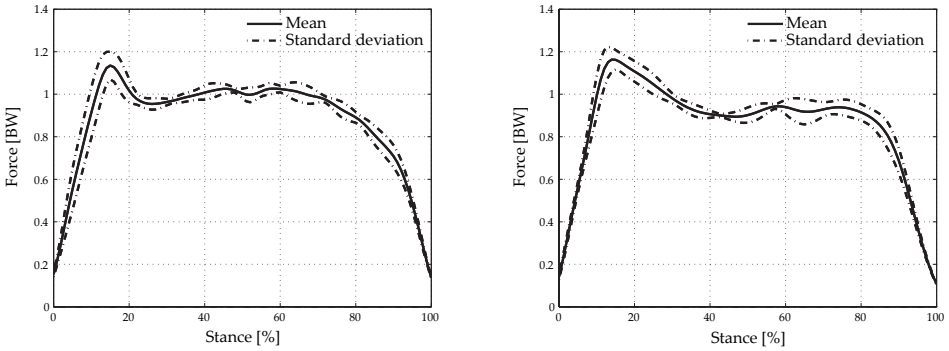

(a) BAPI36 (b) FELE30

Figure 3.7: *Vertical ground reaction force registered for both subjects. Displayed are the mean (continuous line) and the standard deviation (intermittent line) over all the trials.*

3.3 Discussion

The purpose of the measurements was to compare video photogrammetry with video fluoroscopy based stair descent analysis with respect to knee joint kinematics and net moments. Thereby, video fluoroscopic data is regarded as the gold standard.

3.3.1 Knee Joint Kinematics

Ranges of motion at the knee joint are commonly adopted to describe and differentiate healthy from pathological movements [53, 55, 79]. The ranges of motion presented here are in agreement with previous examinations based on video fluoroscopic [9, 33] and video photogrammetric [53, 57, 88] measurements.
In this study, video photogrammetry overestimates the range of motion of adduction-abduction and internal-external rotation and underestimates knee flexion, as previously reported [106]. Significant differences were found between video fluoroscopy and video photogrammetry calculated ranges of motion for flexion-extension and adduction-abduction motion in both subjects. Between subjects, a significant difference could neither be observed among video fluoroscopic nor among video photogrammetric data. Nonetheless, the inter-subject differences of the mean ranges of motion exhibits analog values for both measuring approaches: higher flexion-extension, adduction-abduction and internal-external range of motion were registered for *FELE30* with respect to *BAPI36*. Now, it could be hypothesized that inter-subject anomalies that significantly affect the ranges of motion of the knee joint can be detected equally by both measuring systems. However, this cannot be verified within this study because of the restricted number of involved subjects. Future essays should address and give more insight, whether discrepancies registered in the knee joint ranges of motion by video photogrammetry correlate to those carried out by the underlying structure.
The trajectory pattern of the knee flexion was reproduced fairly well by the video photogrammetric data. However, a consistent offset was noticeable for the flexion angle of *BAPI36*. This is due to the reference position of the extended leg at 0° with respect to the knee arthroplasty reference frame. In other words, if the tibial component was implanted at an angle in the sagittal plane of the knee with respect to the longitudinal axis of the tibia, the flexion that will be registered by the video fluoroscopic system will exhibit an offset at full leg extension.
Adduction-abduction and internal-external rotations calculated by means of video photogrammetric data were not able to reproduce the actual movement of the implant

and exhibited contradictory patterns, as reported in the past for step up/down tasks [41]. This clearly leads to erroneous statements about knee joint kinematics. Studies that try to assess coupling between knee rotations and knee moments or even among knee rotations themselves are inevitably led to wrong conclusions [44, 31, 121]. For any calculation that rely on knee kinematics, such as prediction of knee degenerative patterns [3, 4] or ligament stress calculation [101], significant errors and misleading observations need to be taken into account. Consequently, cautions must be taken when interpreting or utilizing in vivo data gathered exclusively by video photogrammetric systems.

3.3.2 Knee Joint Kinetics

Peak joint moment values, likewise ranges of motion, are utilized to characterize knee joint functionality and to detect eventual disorders [56, 61, 91, 103].
Except for the axial joint moment exhibited by *BAPI36*, there was no significant difference between the peak moments calculated by means of video photogrammetric and video fluoroscopic data. The trajectory pattern of the moments was also closely predicted by the video photogrammetric data. Therefore, it could be assumed that, for knee joint anomalies that affect peak moment values and moment trajectory patterns, video photogrammetry represent a sufficiently accurate measurement tool. However, the system requires an appropriate calibration of the setup as described in chapter 2. Furthermore, the external marker position needs also to be optimized in order to limit soft tissue artifacts, as described in previous studies [69, 107, 106]. Related to the absolute values of the knee joint moments exhibited by both subjects, remarkable differences were found between the two measuring systems throughout most of the stance phase. For instance during the first 10% of stance, an extension moment is yielded by video photogrammetric measurements as opposed to a flexion moment determined by means of video fluoroscopic data. Thus, video photogrammetry can only be used to detect disorders that either correlate to maximal moment generation or qualitatively affect moment trajectories.
Since wrong conclusions about the knee joint kinetics can be drawn by exclusively relying on the data gathered by means of video photogrammetry, it becomes clear that skin marker based gait analysis fails to deliver the accurate data that is essential to understand the mechanisms of the knee joint. Moreover, in order to enhance biomechanical researches of the knee joint, it is inevitable to promote more accurate tools in gait analysis laboratories, such as video fluoroscopy.

3.3.3 Biomechanical Reflections

In this section, only the results calculated by means of video fluoroscopic data are discussed.
The pattern of ground reaction forces in anterior-posterior and vertical direction agree with those reported by other studies [104, 105, 91]. The vertical component exhibited by *BAPI36* shows an initial peek of weight acceptance and a prolonged period during which the vertical ground reaction remains at a constant value of one bodyweight. This can be interpreted as the subject trying to stabilize the center of mass and to minimize vertical accelerations. This can also explain the nearly constant flexion angle during the first third of the stance phase and the more pronounced flexion angle acceleration towards the end of stance, compared to the subject *FELE30*.
During stair descent, an early flexion peak is reported in different studies for normal subjects [55, 83, 91]. For both subject involved in this study, no early peak prior to the maximal peak was detectable in the flexion trajectory. Nonetheless, *FELE30* exhibited a more pronounced deceleration of the knee flexion at 10% of stance, thus indicating a change of flexion toward extension. This was reflected by the first peak observed in the knee extension moment, which shows a resistance to flexion by *FELE30*. However, the extent of the early peak of the extension moment results moderate, when compared to previous studies [35, 56, 77, 91, 95, 103], which reported a more pronounced double waveform in the extension moment trajectory. For the subject *BAPI36*, the early peak was present neither in the flexion angle nor in the extension moment. This indicates a resistance to quadriceps loading [10], which could also explain the relative low maximal extension moment compared to the subject *FELE30*. A similar behavior is reported for subject with knee disabilities [24, 55, 56, 57, 95]. It is argued, that subjects with knee disorders tend to avoid extended loading of the knee during weight acceptance by minimizing the force exerted by the quadriceps muscles, thus reducing the extension moment. Indeed, the subject *BAPI36* claimed about pain during flexion. Now, it could be hypothesized that, over time, the subject developed a compensation pattern to prevent excessive loading, thus limiting pain of the knee joint at pronounced flexion. This was also observed in the extension moment and flexion angle trajectory during the measurements. However, it could also be argued that *BAPI36* lacks the relevant muscle force needed to successfully stabilizes the knee. Therefore, the subject has to perform compensatory movements in order to safely descend the stairs.
Noticeable are also the discrepant patterns of the adduction and internal rotation of the knee joint exhibited by both subjects. *FELE30* exhibited a quite stable pattern throughout the stance phase. It can be reasoned whether the motion of the femur was either primarily restricted by muscle and soft tissue tension at the knee or by a highly

congruent insert. Furthermore, considerable wear of the polyethylene inlay could also induce a limited motion of the femoral component during axial loading. Therefore, a larger movement would only be observed during swing phase where the compressive force acting on the implant component are minimal, as observed in *FELE30*. Moreover, a minor imbalance of the collateral ligaments during knee flexion could lead to the pronounced external rotation and adduction of the femur [38], that was reported during the swing.
In contrast, *BAPI36* did not show such a clear pattern of motion with respect to adduction-abduction and internal-external rotation. It could be argued that the subject has difficulties stabilizing the knee because of a lack in coordination or weak muscles, which would be consistent with the above statement about knee flexion pattern. Evident was the greater inter-trial variability during the swing phase. This could be explained by loose soft tissues at the knee, that fail to properly guide the swinging tibial with respect to femoral component.

Get the habit of analysis —
Analysis will in time enable synthesis to become your habit of mind.

Frank Lloyd Wright (1867-1959)

4

Synthesis

Profound understanding of the mechanisms in the knee joint is essential for the development and optimization of new total knee replacement designs. Moreover, problematic motion tasks need to be first discerned and then extensively analyzed. Stair descent falls in this category.
Consequently, the main goal of this thesis was to gather accurate data of in vivo kinematics and kinetics of total knee joint replacement during stair descent.

The first step was to enhance the automated moving fluoroscopic system to track the knee during level walking. At the beginning of this thesis, the ability to track the knee joint by the existing prototype was limited to slow walking speed. During level gait, the automated fluoroscope managed to keep the center of the knee in the field of view of the imaging system exclusively for the stance phase. In other words, the system was not able to accelerate fast enough to keep up with the dynamic motion of the knee during the entire gait cycle. Therefore, a new horizontal drive assembly was developed, which enabled to track the knee joint during several consecutive gait cycles.
In a second step, the automated fluoroscope was upgraded to follow the knee during stair descent. Since the vertical movement of the knee during the stance phase of stair descent is correlated to the step size, the fluoroscopic C-arm needed to be moved vertically. Consequently, a new concept was developed for the fixation of the C-arm. Two motorized linear guides were installed and synchronized to provide a smooth motion of the system. By upgrading the knee position sensor for two dimensional measurement, the new automated moving fluoroscope was able to track the knee

during stair descent, step transition and level walking at once.

The third step was to enhance the quality of the fluoroscopic imaging system. Previous studies on the premises revealed that poor image quality negatively affected the evaluation of the three dimensional pose of the implant components. Therefore, a new CCD sensor was installed. This rendered clearer images and allowed to access and optimize the imaging parameters directly. Moreover, the new assembly implicated the modification of the entire image processing chain. Image distortion correction, projection parameter estimation and implant registration were in part totally revised. Consequently, the accuracy of the 2D to 3D registration algorithm had to be revaluated. The results of the error assessment revealed an improvement of the accuracy of the implant pose estimation up to two times. However, the registration algorithm turned out to be quite sensitive to implant volume deviations from the original computer aided design model. Therefore, special care has to be taken with respect to the volumetric data definition that is used to estimate the implant pose. As a worst case scenario, an overall surface deviation of a tenth of millimeters would result in an out-of-plane pose estimation error of a couple of millimeters.

The fourth step consisted in developing an instrumented staircase and in defining a calibration for the force vector orientation.
Two mobile force plates were installed in two consecutive steps of the staircase. In order to avoid a cross-talk between the dynamic motion carried out by the automated fluoroscopic equipment and the force measurement signals, the staircase was designed to fit on top of the fixed force plates of the gait laboratory. This ensured a mechanical isolation of the force measurements with respect to the surrounding floor.
With respect to knee joint moment calculation, an improvement of the kinematic measurements makes only sense, when the kinetic data acquisition is accordingly calibrated. Therefore, the crosstalk between the force measurement components needed to be evaluated.
A time varying force was conveyed at 66 predefined points on the surface of the plate, while the direction of the applied force was simultaneously registered. By means of an optimization algorithm, the error of the measured force orientation was reduced by approximately 50%.

The final step comprised the in vivo kinematic and kinetic acquisition of a total knee joint replacement during stair descent. The results calculated by means of video photogrammetry data were subsequently compared to video fluoroscopic measurements. Video fluoroscopy was defined as the gold standard.
Two subject were recruited for the present study. Knee joint rotations and moments

were calculated for each subject. The results showed that video photogrammetric measurements returned contradictive trajectories for adduction-abduction and internal-external rotations in both subjects. Therefore, erroneous statements are very likely to occur, when the observations rely exclusively on kinematic data gathered by means of external skin mounted markers.
Although peek knee joint moments were well reproduced by video photogrammetric data, the absolute values of the moments differed remarkably from calculations based on video fluoroscopic acquisitions. Therefore, it was concluded, that it is safe to utilize video photogrammetry in order to detect knee disorders that correlate to maximal moment generation, provided that the system has been enhanced, e.g. by means of force plate calibration and choice of an optimal external marker cluster. However, measurements which exclusively depend on external skin mounted markers fail to deliver accurate data for an extensive biomechanical analysis of the knee joint.

4.1 Outlook

The present work shows the limitations of conventional gait analysis and promotes a more accurate measurement approach to determine knee joint mechanics. Thereby, the focus was mainly concentrated to the analysis of stair descent, which is one of the greatest sources of knee joint discomfort during daily activities.
To which extent this trivial, yet strenuous, motion task affects the kinematics and kinetics of total knee replacements was still to be clarified. However, during this thesis, instability motion patterns could be well observed for the subject that claimed about flexion difficulties. This finding was accompanied by an obvious overall reduction of the flexion moment. Therefore, it can be argued that the measuring setup developed during this thesis provides a measuring tool to not only detect, but also to accurately observe and analyze pathological motion patterns. This could definitely bring new and deeper insight as well as useful understanding of the correlation of pathological knee mechanics to the causes, why certain knee arthroplasty designs fail, or even give certain indications of what need to be changed in the whole replacement procedures, from design planning to rehabilitation programs, in order to achieve a better patient outcome.
Certainly, this measurement system alone will not give the only and final answer to all the questions that arise with respect to knee replacement failure, but gives new possibilities for new and thorough studies in order to clarify the reasons that lead to patient discomforts with respect to knee mechanics.

Bibliography

[1] E. J. Alexander and T. P. Andriacchi. Correcting for deformation in skin-based marker systems. *J Biomech*, 34(3):355–61, 2001.

[2] T. P. Andriacchi, E. J. Alexander, M. K. Toney, C. Dyrby, and J. Sum. A point cluster method for in vivo motion analysis: applied to a study of knee kinematics. *J Biomech Eng*, 120(6):743–9, 1998.

[3] T. P. Andriacchi and C. O. Dyrby. Interactions between kinematics and loading during walking for the normal and acl deficient knee. *J Biomech*, 38(2):293–8, 2005.

[4] T. P. Andriacchi, C. O. Dyrby, and T. S. Johnson. The use of functional analysis in evaluating knee kinematics. *Clin Orthop Relat Res*, (410):44–53, 2003.

[5] T. P. Andriacchi and J. O. Galante. Retention of the posterior cruciate in total knee arthroplasty. *J Arthroplasty*, 3 Suppl:S13–9, 1988.

[6] T. P. Andriacchi, J. O. Galante, and R. W. Fermier. The influence of total knee-replacement design on walking and stair-climbing. *J Bone Joint Surg Am*, 64(9):1328–35, 1982.

[7] J. Arima, L. A. Whiteside, J. W. Martin, H. Miura, S. E. White, and D. S. McCarthy. Effect of partial release of the posterior cruciate ligament in total knee arthroplasty. *Clin Orthop Relat Res*, (353):194–202, 1998.

[8] W.S. Baer. Arthroplasty with the aid of animal membrane. *Am J Orhop Surg*, (16):1–29, 1918.

[9] S. A. Banks, G. D. Markovich, and W. A. Hodge. In vivo kinematics of cruciate-retaining and -substituting knee arthroplasties. *J Arthroplasty*, 12(3):297–304, 1997.

[10] M. Berchuck, T. P. Andriacchi, B. R. Bach, and B. Reider. Gait adaptations by patients who have a deficient anterior cruciate ligament. *J Bone Joint Surg Am*, 72(6):871–7, 1990.

[11] R. A. Berger, A. G. Rosenberg, R. M. Barden, M. B. Sheinkop, J. J. Jacobs, and J. O. Galante. Long-term followup of the miller-galante total knee replacement. *Clin Orthop Relat Res*, (388):58–67, 2001.

[12] J. E. Brown, Gaw Wh Mc, and D. T. Shaw. Use of cutis as an interposing membrane in arthroplasty of the knee. *J Bone Joint Surg Am*, 40-A(5):1003–18, 1958.

[13] F. F. Buechel and M. J. Pappas. The new jersey low-contact-stress knee replacement system: biomechanical rationale and review of the first 123 cemented cases. *Arch Orthop Trauma Surg*, 105(4):197–204, 1986.

[14] Sr. Buechel, F. F., Jr. Buechel, F. F., M. J. Pappas, and J. D'Alessio. Twenty-year evaluation of meniscal bearing and rotating platform knee replacements. *Clin Orthop Relat Res*, (388):41–50, 2001.

[15] K. V. Burckhardt. *Locating implants with respect to the bone in diagnostic X-ray images of the pelvis*. Dissertation, ETH, 2001.

[16] W. C. Campbell. Interposition of vitallium plates in arthroplasties of the knee: Preliminary report. *Clin Orthop Relat Res*, (120):4–6, 1976.

[17] A. Cappozzo, A. Cappello, U. Della Croce, and F. Pensalfini. Surface-marker cluster design criteria for 3-d bone movement reconstruction. *IEEE Trans Biomed Eng*, 44(12):1165–74, 1997.

[18] A. Cappozzo, U. D. Croce, A. Leardini, and L. Chiari. Human movement analysis using stereophotogrammetry. part 1: theoretical background. *Gait Posture*, 21(2):186–96, 2005.

[19] C. A. Carpenter and T. S. Thronhill. Posterior cruciate ligament retention in total knee replacement. In *The Adult Knee*, volume 2, pages 1135–44. Linppincott Williams and Wilkins, Philadelphia, 1st edition, 2003.

[20] L. Chiari, U. D. Croce, A. Leardini, and A. Cappozzo. Human movement analysis using stereophotogrammetry. part 2: instrumental errors. *Gait Posture*, 21(2):197–211, 2005.

[21] K. A. Christina and P. R. Cavanagh. Ground reaction forces and frictional demands during stair descent: effects of age and illumination. *Gait Posture*, 15(2):153–8, 2002.

[22] W. A. Colizza, J. N. Insall, and G. R. Scuderi. The posterior stabilized total knee prosthesis. assessment of polyethylene damage and osteolysis after a ten-year-minimum follow-up. *J Bone Joint Surg Am*, 77(11):1713–20, 1995.

[23] U. D. Croce, A. Leardini, L. Chiari, and A. Cappozzo. Human movement analysis using stereophotogrammetry. part 4: assessment of anatomical landmark misplacement and its effects on joint kinematics. *Gait Posture*, 21(2):226–37, 2005.

[24] K. M. Crossley, S. M. Cowan, K. L. Bennell, and J. McConnell. Knee flexion during stair ambulation is altered in individuals with patellofemoral pain. *J Orthop Res*, 22(2):267–74, 2004.

[25] A. Deburge and Guepar. Guepar hinge prosthesis: complications and results with two years' follow-up. *Clin Orthop Relat Res*, (120):47–53, 1976.

[26] D. Dejour, G. Deschamps, L. Garotta, and H. Dejour. Laxity in posterior cruciate sparing and posterior stabilized total knee prostheses. *Clin Orthop Relat Res*, (364):182–93, 1999.

[27] D. A. Dennis, R. D. Komistek, Jr. Colwell, C. E., C. S. Ranawat, R. D. Scott, T. S. Thornhill, and M. A. Lapp. In vivo anteroposterior femorotibial translation of total knee arthroplasty: a multicenter analysis. *Clin Orthop Relat Res*, (356):47–57, 1998.

[28] D. A. Dennis, R. D. Komistek, and M. R. Mahfouz. In vivo fluoroscopic analysis of fixed-bearing total knee replacements. *Clin Orthop Relat Res*, (410):114–30, 2003.

[29] D. A. Dennis, M. R. Mahfouz, R. D. Komistek, and W. Hoff. In vivo determination of normal and anterior cruciate ligament-deficient knee kinematics. *J Biomech*, 38(2):241–53, 2005.

[30] M. T. Dettwyler. *Biomechanische Untersuchungen und Modellierungen am menschlichen oberen Sprunggelenk im Hinblick auf Arthroplastiken*. Dissertation, ETH, 2005.

[31] B. el Nahass, M. M. Madson, and P. S. Walker. Motion of the knee after condylar resurfacing–an in vivo study. *J Biomech*, 24(12):1107–17, 1991.

[32] S. Fantozzi, M. G. Benedetti, A. Leardini, S. A. Banks, A. Cappello, D. Assirelli, and F. Catani. Fluoroscopic and gait analysis of the functional performance in

stair ascent of two total knee replacement designs. *Gait Posture*, 17(3):225–34, 2003.

[33] S. Fantozzi, F. Catani, A. Ensini, A. Leardini, and S. Giannini. Femoral rollback of cruciate-retaining and posterior-stabilized total knee replacements: in vivo fluoroscopic analysis during activities of daily living. *J Orthop Res*, 24(12):2222–9, 2006.

[34] W. Ferguson. Excision of knee joint: recovery with a false joint and a useful limb. *Med Times Gazette*, 1:601, 1861.

[35] D. Beaulieu FG, L. Pelland, and D. G. Robertson. Kinetic analysis of forwards and backwards stair descent. *Gait Posture*, 27(4):564–71, 2008.

[36] M. Foresti, H. Gerber, and E. Stuessi. Automated moving fluoroscope: a novel method to acquire video fluoroscopic data during level walking. *Journal of Biomechanics*, 39(Supplement 1):S109–S109, 2006.

[37] M. Foresti, H. Gerber, and E. Stuessi. Biomechanics of the knee by means of a two degrees of freedom automated video fluoroscope and instrumented stairs. In *8th International Symposium on Computer Methods in Biomechanics and Biomedical Engineering*, Porto, Portugal, 2008.

[38] M. Foresti, H. Gerber, and E. Stuessi. Axis of rotation of a posterior cruciate retaining total knee arthroplasty during stair descent. In *Knee Arthroplasty 2009: From early intervention to revision*, London, 2009.

[39] M. Foresti, H. Gerber, M. S. Zihlmann, and E. Stuessi. A novel set-up for the automation of a video fluoroscope to retrieve in vivo knee joint kinematics during level walking. In *9th Symposium On 3D Analysis Of Human Movement*, Valenciennе, France, 2006.

[40] M. A. Freeman and V. Pinskerova. The movement of the normal tibio-femoral joint. *J Biomech*, 38(2):197–208, 2005.

[41] E. H. Garling, B. L. Kaptein, B. Mertens, W. Barendregt, H. E. Veeger, R. G. Nelissen, and E. R. Valstar. Soft-tissue artefact assessment during step-up using fluoroscopy and skin-mounted markers. *J Biomech*, 40 Suppl 1:S18–24, 2007.

[42] G. S. Gill and A. B. Joshi. Long-term results of kinematic condylar knee replacement. an analysis of 404 knees. *J Bone Joint Surg Br*, 83(3):355–8, 2001.

[43] J. Goodfellow and J. O'Connor. The mechanics of the knee and prosthesis design. *J Bone Joint Surg Br*, 60-B(3):358–69, 1978.

[44] E. S. Grood, S. F. Stowers, and F. R. Noyes. Limits of movement in the human knee. effect of sectioning the posterior cruciate ligament and posterolateral structures. *J Bone Joint Surg Am*, 70(1):88–97, 1988.

[45] F. H. Gunston. Polycentric knee arthroplasty. prosthetic simulation of normal knee movement. *J Bone Joint Surg Br*, 53(2):272–7, 1971.

[46] D. E. Hardt and R. W. Mann. A five body–three dimensional dynamic analysis of walking. *J Biomech*, 13(5):455–7, 1980.

[47] C. D. Harner, G. H. Baek, T. M. Vogrin, G. J. Carlin, S. Kashiwaguchi, and S. L. Woo. Quantitative analysis of human cruciate ligament insertions. *Arthroscopy*, 15(7):741–9, 1999.

[48] C. D. Harner, J. W. Xerogeanes, G. A. Livesay, G. J. Carlin, B. A. Smith, T. Kusayama, S. Kashiwaguchi, and S. L. Woo. The human posterior cruciate ligament complex: an interdisciplinary study. ligament morphology and biomechanical evaluation. *Am J Sports Med*, 23(6):736–45, 1995.

[49] R. Hartley and A. Zisserman. *Multiple View Geometry in Computer Vision*. Cambridge University Press, Cambridge, 2000.

[50] K. T. Heaton and L. D. Dorr. History of total knee arthroplasty. In *The Adult Knee*, volume 1. Lippincott Williams and Wilkins, 2003.

[51] F. Helfreich. Geschichte der chirurgie. In Fischer, editor, *Handbuch der Geschichte der Medizin*, volume 3. Neuere Zeit, Jena, 1905.

[52] A. L. Hof. An explicit expression for the moment in multibody systems. *J Biomech*, 25(10):1209–11, 1992.

[53] T. Hortobagyi, C. Mizelle, S. Beam, and P. DeVita. Old adults perform activities of daily living near their maximal capabilities. *J Gerontol A Biol Sci Med Sci*, 58(5):M453–60, 2003.

[54] J. Insall, C. S. Ranawat, W. N. Scott, and P. Walker. Total condylar knee replacment: preliminary report. *Clin Orthop Relat Res*, (120):149–54, 1976.

[55] S. Iwata, Y. Suda, T. Nagura, H. Matsumoto, T. Otani, T. P. Andriacchi, and Y. Toyama. Clinical disability in posterior cruciate ligament deficient patients does not relate to knee laxity, but relates to dynamic knee function during stair descending. *Knee Surg Sports Traumatol Arthrosc*, 15(4):335–42, 2007.

[56] S. Iwata, Y. Suda, T. Nagura, H. Matsumoto, T. Otani, and Y. Toyama. Dynamic instability during stair descent in isolated pcl-deficient knees: what affects abnormal posterior translation of the tibia in pcl-deficient knees? *Knee Surg Sports Traumatol Arthrosc*, 15(6):705–11, 2007.

[57] D. S. Jevsevar, P. O. Riley, W. A. Hodge, and D. E. Krebs. Knee kinematics and kinetics during locomotor activities of daily living in subjects with knee arthroplasty and in healthy control subjects. *Phys Ther*, 73(4):229–39; discussion 240–2, 1993.

[58] H. Johansson, P. Sjolander, and P. Sojka. Receptors in the knee joint ligaments and their role in the biomechanics of the joint. *Crit Rev Biomed Eng*, 18(5):341–68, 1991.

[59] R. D. Komistek, D. A. Dennis, and M. Mahfouz. In vivo fluoroscopic analysis of the normal human knee. *Clin Orthop Relat Res*, (410):69–81, 2003.

[60] R. D. Komistek, T. R. Kane, M. Mahfouz, J. A. Ochoa, and D. A. Dennis. Knee mechanics: a review of past and present techniques to determine in vivo loads. *J Biomech*, 38(2):215–28, 2005.

[61] D. L. Kowalk, J. A. Duncan, and C. L. Vaughan. Abduction-adduction moments at the knee during stair ascent and descent. *J Biomech*, 29(3):383–8, 1996.

[62] B. Krabbe, R. Farkas, and W. Baumann. Influence of inertia on intersegment moments of the lower extremity joints. *J Biomech*, 30(5):517–9, 1997.

[63] J. G. Kuhns and T. A. Potter. Nylon arthroplasty of the knee joint in chronic arthritis. *Surg Gynecol Obstet*, 91(3):351–62, 1950.

[64] M. A. Lafortune, P. R. Cavanagh, 3rd Sommer, H. J., and A. Kalenak. Three-dimensional kinematics of the human knee during walking. *J Biomech*, 25(4):347–57, 1992.

[65] M. A. Lafortune, E. Henning, and G. A. Valiant. Tibial shock measured with bone and skin mounted transducers. *J Biomech*, 28(8):989–93, 1995.

[66] M. A. Lafortune, M. J. Lake, and E. Hennig. Transfer function between tibial acceleration and ground reaction force. *J Biomech*, 28(1):113–7, 1995.

[67] R. S. Laskin and H. M. O'Flynn. The insall award. total knee replacement with posterior cruciate ligament retention in rheumatoid arthritis. problems and complications. *Clin Orthop Relat Res*, (345):24–8, 1997.

[68] A. Leardini, L. Chiari, U. D. Croce, and A. Cappozzo. Human movement analysis using stereophotogrammetry. part 3. soft tissue artifact assessment and compensation. *Gait Posture*, 21(2):212–25, 2005.

[69] R. List. *A Hybrid Marker Set. For Future Basic Research and Instrumented Gait Analysis at the Laboratory for Biomechanics*. Master thesis, ETH Zurich, 2005.

[70] L. Lucchetti, A. Cappozzo, A. Cappello, and U. Della Croce. Skin movement artefact assessment and compensation in the estimation of knee-joint kinematics. *J Biomech*, 31(11):977–84, 1998.

[71] W.R. Mac Ausland. Knee joint arthroplasty. *J Am Med Assoc*, (101):1699–1702, 1933.

[72] M. R. Mahfouz, W. A. Hoff, R. D. Komistek, and D. A. Dennis. A robust method for registration of three-dimensional knee implant models to two-dimensional fluoroscopy images. *IEEE Trans Med Imaging*, 22(12):1561–74, 2003.

[73] M. R. Mahfouz, R. D. Komistek, D. A. Dennis, and W. A. Hoff. In vivo assessment of the kinematics in normal and anterior cruciate ligament-deficient knees. *J Bone Joint Surg Am*, 86-A Suppl 2:56–61, 2004.

[74] M. R. Mahfouz, S. M. Traina, R. D. Komistek, and D. A. Dennis. In vivo determination of knee kinematics in patients with a hamstring or patellar tendon acl graft. *J Knee Surg*, 16(4):197–202, 2003.

[75] K. Manal, I. McClay, S. Stanhope, J. Richards, and B. Galinat. Comparison of surface mounted markers and attachment methods in estimating tibial rotations during walking: an in vivo study. *Gait Posture*, 11(1):38–45, 2000.

[76] A. Matsas, N. Taylor, and H. McBurney. Knee joint kinematics from familiarised treadmill walking can be generalised to overground walking in young unimpaired subjects. *Gait Posture*, 11(1):46–53, 2000.

[77] B. J. McFadyen and D. A. Winter. An integrated biomechanical analysis of normal stair ascent and descent. *J Biomech*, 21(9):733–44, 1988.

[78] O. S. Mian, M. V. Narici, A. E. Minetti, and V. Baltzopoulos. Centre of mass motion during stair negotiation in young and older men. *Gait Posture*, 26(3):463–9, 2007.

[79] O. S. Mian, J. M. Thom, M. V. Narici, and V. Baltzopoulos. Kinematics of stair descent in young and older adults and the impact of exercise training. *Gait Posture*, 25(1):9–17, 2007.

[80] J. B. Murphy. The classic: ankylosis: arthroplasty–clinical and experimental. 1905. *Clin Orthop Relat Res*, 466(11):2573–8, 2008.

[81] M. P. Murray, G. B. Spurr, S. B. Sepic, G. M. Gardner, and L. A. Mollinger. Treadmill vs. floor walking: kinematics, electromyogram, and heart rate. *J Appl Physiol*, 59(1):87–91, 1985.

[82] M. W. Pagnano, A. D. Hanssen, D. G. Lewallen, and M. J. Stuart. Flexion instability after primary posterior cruciate retaining total knee arthroplasty. *Clin Orthop Relat Res*, (356):39–46, 1998.

[83] A. Protopapadaki, W. I. Drechsler, M. C. Cramp, F. J. Coutts, and O. M. Scott. Hip, knee, ankle kinematics and kinetics during stair ascent and descent in healthy young individuals. *Clin Biomech (Bristol, Avon)*, 22(2):203–10, 2007.

[84] A. Race and A. A. Amis. The mechanical properties of the two bundles of the human posterior curciate ligament. *J Biomech*, 27(1):13–24, 1994.

[85] E. L. Radin and I. L. Paul. Response of joints to impact loading. i. in vitro wear. *Arthritis Rheum*, 14(3):356–62, 1971.

[86] C. S. Ranawat, R. D. Komistek, J. A. Rodriguez, D. A. Dennis, and M. Anderle. In vivo kinematics for fixed and mobile-bearing posterior stabilized knee prostheses. *Clin Orthop Relat Res*, (418):184–90, 2004.

[87] Rauber and Kopsch. *Bewegungsapparat*, volume 1 of *Anatomie des Menschen*. Georg Thieme Verlag Stuttgart, 1987.

[88] N. D. Reeves, M. Spanjaard, A. A. Mohagheghi, V. Baltzopoulos, and C. N. Maganaris. The demands of stair descent relative to maximum capacities in elderly and young adults. *J Electromyogr Kinesiol*, 18(2):218–27, 2008.

[89] C. Reinschmidt, A. J. van den Bogert, A. Lundberg, B. M. Nigg, N. Murphy, A. Stacoff, and A. Stano. Tibiofemoral and tibiocalcaneal motion during walking: external vs. skeletal markers. *Gait Posture*, 6:98–109, 1996.

[90] C. Reinschmidt, A. J. van den Bogert, B. M. Nigg, A. Lundberg, and N. Murphy. Effect of skin movement on the analysis of skeletal knee joint motion during running. *J Biomech*, 30(7):729–32, 1997.

[91] R. Riener, M. Rabuffetti, and C. Frigo. Stair ascent and descent at different inclinations. *Gait Posture*, 15(1):32–44, 2002.

[92] M. A. Ritter, P. M. Faris, and E. M. Keating. Posterior cruciate ligament balancing during total knee arthroplasty. *J Arthroplasty*, 3(4):323–6, 1988.

[93] J. R. Robinson, J. Sanchez-Ballester, A. M. Bull, W. Thomas Rde, and A. A. Amis. The posteromedial corner revisited. an anatomical description of the passive restraining structures of the medial aspect of the human knee. *J Bone Joint Surg Br*, 86(5):674–81, 2004.

[94] T. Saari, R. Tranberg, R. Zugner, J. Uvehammer, and J. Karrholm. Total knee replacement influences both knee and hip joint kinematics during stair climbing. *Int Orthop*, 28(2):82–6, 2004.

[95] G. B. Salsich, J. H. Brechter, and C. M. Powers. Lower extremity kinetics during stair ambulation in patients with and without patellofemoral pain. *Clin Biomech (Bristol, Avon)*, 16(10):906–12, 2001.

[96] J. E. Samson. Arthroplasty of the knee joint; late results. *J Bone Joint Surg Am*, 31B(1):50–2, 1949.

[97] P. A. Schai, T. S. Thornhill, and R. D. Scott. Total knee arthroplasty with the pfc system. results at a minimum of ten years and survivorship analysis. *J Bone Joint Surg Br*, 80(5):850–8, 1998.

[98] R. D. Scott and T. S. Thornhill. Posterior cruciate supplementing total knee replacement using conforming inserts and cruciate recession. effect on range of motion and radiolucent lines. *Clin Orthop Relat Res*, (309):146–9, 1994.

[99] G. R. Scuderi, J. N. Insall, R. E. Windsor, and M. C. Moran. Survivorship of cemented knee replacements. *J Bone Joint Surg Br*, 71(5):798–803, 1989.

[100] G. S. Sextro, D. J. Berry, and J. A. Rand. Total knee arthroplasty using cruciate-retaining kinematic condylar prosthesis. *Clin Orthop Relat Res*, (388):33–40, 2001.

[101] K. B. Shelburne, M. G. Pandy, F. C. Anderson, and M. R. Torry. Pattern of anterior cruciate ligament force in normal walking. *J Biomech*, 37(6):797–805, 2004.

[102] S. Simmons, S. Lephart, H. Rubash, P. Borsa, and R. L. Barrack. Proprioception following total knee arthroplasty with and without the posterior cruciate ligament. *J Arthroplasty*, 11(7):763–8, 1996.

[103] M. Spanjaard, N. D. Reeves, J. H. van Dieen, V. Baltzopoulos, and C. N. Maganaris. Lower-limb biomechanics during stair descent: influence of step-height and body mass. *J Exp Biol*, 211(Pt 9):1368–75, 2008.

[104] A. Stacoff, C. Diezi, G. Luder, E. Stuessi, and I. A. Kramers-de Quervain. Ground reaction forces on stairs: effects of stair inclination and age. *Gait Posture*, 21(1):24–38, 2005.

[105] A. Stacoff, I. A. Kramers-de Quervain, G. Luder, R. List, and E. Stussi. Ground reaction forces on stairs. part ii: knee implant patients versus normals. *Gait Posture*, 26(1):48–58, 2007.

[106] R. Stagni, S. Fantozzi, A. Cappello, and A. Leardini. Quantification of soft tissue artefact in motion analysis by combining 3d fluoroscopy and stereophotogrammetry: a study on two subjects. *Clin Biomech (Bristol, Avon)*, 20(3):320–9, 2005.

[107] R. Stagni, A. Leardini, A. Cappozzo, M. Grazia Benedetti, and A. Cappello. Effects of hip joint centre mislocation on gait analysis results. *J Biomech*, 33(11):1479–87, 2000.

[108] S. H. Stern and J. N. Insall. Posterior stabilized prosthesis. results after follow-up of nine to twelve years. *J Bone Joint Surg Am*, 74(7):980–6, 1992.

[109] J. B. Stiehl, R. D. Komistek, D. A. Dennis, R. D. Paxson, and W. A. Hoff. Fluoroscopic analysis of kinematics after posterior-cruciate-retaining knee arthroplasty. *J Bone Joint Surg Br*, 77(6):884–9, 1995.

[110] G. M. Strathy, E. Y. Chao, and R. K. Laughman. Changes in knee function associated with treadmill ambulation. *J Biomech*, 16(7):517–22, 1983.

[111] E. Stuessi and H. U. Debrunner. Parameter-analyse des menschlichen ganges. *Biomed Tech*, 25:222–224, 1980.

[112] C. Townley and L. Hill. Total knee replacement. *Am J Nurs*, 74(9):1612–7, 1974.

[113] A.J. Tria and K.S. Klein. *An illustrated guide to the knee*. Churchill Livingstone, New York, 1 edition, 1992.

[114] A. Verneuil. De la creation d'une fausse articulation par section ou resection partielle de l'os maxillaire inferieur, comme moyen de remedier a l'ankylose vraie ou fausse de la machoire inferieure. *Arch Gen Med*, (15):174, 1860.

[115] B. Walldius. Arthroplasty of the knee with an endoprosthesis. *Acta Chir Scand*, 113(6):445–6, 1957.

[116] P. J. Warren, T. K. Olanlokun, A. G. Cobb, and G. Bentley. Proprioception after knee arthroplasty. the influence of prosthetic design. *Clin Orthop Relat Res*, (297):182–7, 1993.

[117] R. L. Worland, D. E. Jessup, and J. Johnson. Posterior cruciate recession in total knee arthroplasty. *J Arthroplasty*, 12(1):70–3, 1997.

[118] T.M. Wright. Knee biomechanics and implant design. In *The Adult Knee*, volume 1, page 145. Lippincott Williams and Wilkins, Philadelphia, 2003.

[119] G. Wu and Z. Ladin. Limitations of quasi-static estimation of human joint loading during locomotion. *Med Biol Eng Comput*, 34(6):472–6, 1996.

[120] B. Yu, T. Kienbacher, E. S. Growney, M. E. Johnson, and K. N. An. Reproducibility of the kinematics and kinetics of the lower extremity during normal stair-climbing. *J Orthop Res*, 15(3):348–52, 1997.

[121] B. Yu, M. J. Stuart, T. Kienbacher, E. S. Growney, and K. N. An. Valgus-varus motion of the knee in normal level walking and stair climbing. *Clin Biomech (Bristol, Avon)*, 12(5):286–293, 1997.

[122] M. S. Zihlmann. *Total knee arthroplasty biomechanical reflections and modelling, based on quantitative movement analysis*. Dissertation, ETH, 2005.

[123] M. S. Zihlmann, H. Gerber, A. Stacoff, K. Burckhardt, G. Szekely, and E. Stuessi. Three-dimensional kinematics and kinetics of total knee arthroplasty during level walking using single plane video-fluoroscopy and force plates: a pilot study. *Gait Posture*, 24(4):475–81, 2006.

Mauro Foresti

Curriculum vitae

Education

2005 – now **PhD. Student**, *Institute for Biomechanics, ETH Zurich*, Zurich.

1997 – 2002 **Dipl. El.-Ing. ETH**, *ETH Zurich*, Zurich.
Diploma Thesis
title *Channel Estimation and Adaptive Techniques for MIMO OFDM Systems*
supervisors Dr. Carlo Mutti, Prof. Dr. Dirk Dahlhaus

1993 – 1994 **Graduation year**, *Mio Au Sable High School*, Mio, USA.

1991 – 1996 **Matura**, *Kollegium Kantonsschule Schwyz*, Schwyz.

Experience

Vocational

2003 – now **Research Assistant**, *Institute for Biomechanics, ETH Zurich*, Zurich.
System Administration, Software and Hardware Development, Lecturer

2001 **Research Assistant**, *Helsinki University of Technology*, Helsinki, Finland.
DSP Application Development

Miscellaneous

1999 – 2001 **Teaching Assistant**, *ETH Zurich*, Zurich.
Mechanics, Signal & Systems, Digital Signalprocessing

1998 – 1999 **Teaching Assistant**, *Private School DeBeer Lerncenter*, Zurich.
Physics, Mathematics

Publications and Conference Abstracts

M. Foresti, H. Gerber, and E. Stuessi. Automated moving fluoroscope: a novel method to acquire video fluoroscopic data during level walking. *Journal of Biomechanics*, 39(Supplement 1):S109–S109, 2006.

M. Foresti, H. Gerber, and E. Stuessi. Biomechanics of the knee by means of a two degrees of freedom automated video fluoroscope and instrumented stairs. In *8th International Symposium on Computer Methods in Biomechanics and Biomedical Engineering*, Porto, Portugal, 2008.

M. Foresti, H. Gerber, and E. Stuessi. 3d kinematics of a total knee arthroplasty during stair descent: video-photogrammetry vs. video-fluoroscopy. In *XXII Congress of the International Society of Biomechanics*, Cape Town, South Africa, 2009.

M. Foresti, H. Gerber, and E. Stuessi. Axis of rotation of a posterior cruciate retaining total knee arthroplasty during stair descent. In *Knee Arthroplasty 2009: From early intervention to revision*, London, 2009.

M. Foresti, H. Gerber, M. S. Zihlmann, and E. Stuessi. A novel set-up for the automation of a video fluoroscope to retrieve in vivo knee joint kinematics during level walking. In *9th Symposium On 3D Analysis Of Human Movement*, Valencienne, France, 2006.

H. Gerber, M. Foresti, M. Zihlmann, and E. Stuessi. Method to simultaneously measure kinetic and 3d kinematic data during normal level walking using kistler force plates, vicon system and video-fluoroscopy. *Journal of Biomechanics*, 40(Supplement 2):S405–S405, 2007.

H. Gerber, M. S. Zihlmann, M. Foresti, and E. Stussi. Method to simultaneously measure 3d kinematic and kinetic data during normal level walking using kistler force plates, vicon system and video-fluoroscopy. In *9th Symposium On 3D Analysis Of Human Movement*, Valencienne, France, 2006.

R. List, M. Foresti, H. Gerber, and E. Stuessi. 3d kinematics of ankle arthroplasties using videofluoroscopy. In *XXII Congress of the International Society of Biomechanics*, Cape Town, South Africa, 2009.

R. List, A. Stacoff, M. Foresti, H. Gerber, and E. Stuessi. An in vivo procedure to quantify 3d kinematics of ankle arthroplasties using videofluoroscopy. *Journal of Biomechanics*, 41(Supplement 1):S321, 2008.

C. Mutti, D. Dahlhaus, T. Hunziker, and M. Foresti. Bit and power loading procedures for ofdm systems with bit-interleaved coded modulation. *Ict'2003: 10th International Conference on Telecommunications, Vols I and II, Conference Proceedings*, pages 1422–1427 1779, 2003.